Grotzinger J. P., Hayes A. G., Lamb M. P., and McLennan S. M. (2013) Sedimentary processes on Earth, Mars, Titan, and Venus. In *Comparative Climatology of Terrestrial Planets* (S. J. Mackwell et al., eds.), pp. 439–472. Univ. of Arizona, Tucson, DOI: 10.2458/azu_uapress_9780816530595-ch18.

Sedimentary Processes on Earth, Mars, Titan, and Venus

J. P. Grotzinger
California Institute of Technology

A. G. Hayes
Cornell University

M. P. Lamb
California Institute of Technology

S. M. McLennan
State University of New York at Stony Brook

The production, transport and deposition of sediment occur to varying degrees on Earth, Mars, Venus, and Titan. These sedimentary processes are significantly influenced by climate that affects production of sediment in source regions (weathering), and the mode by which that sediment is transported (wind vs. water). Other, more geological, factors determine where sediments are deposited (topography and tectonics). Fluvial and marine processes dominate Earth both today and in its geologic past, aeolian processes dominate modern Mars although in its past fluvial processes also were important, Venus knows only aeolian processes, and Titan shows evidence of both fluvial and aeolian processes. Earth and Mars also feature vast deposits of sedimentary rocks, spanning billions of years of planetary history. These ancient rocks preserve the long-term record of the evolution of surface environments, including variations in climate state. On Mars, sedimentary rocks record the transition from wetter, neutral-pH weathering, to brine-dominated low-pH weathering, to its dry current state.

1. INTRODUCTION

The atmospheres of solid planets exert a fundamental control on their surfaces. Interactions between atmospheric and geologic processes influence the morphology and composition of surfaces, and over the course of geologic time determine the historical evolution of the planet's surface environments including climate. In the case of Earth, the origin of life likely occurred within surface environments that were tuned to favor prebiotic chemical reactions. Microbial evolution and the advent of oxygenic photosynthesis created Earth's unique atmospheric fingerprint that would be visible from other solar systems.

Earth, Mars, Venus, and Titan are examples of solid planets that have relatively dense atmospheres (Table 1). Yet each planet has shown divergent evolution over the course of geologic history, and their atmospheres are a testimony to this evolution. A second manifestation of this evolution is preserved in each planet's sedimentary record. Processes that operate at planetary surfaces have the potential to record a history of their evolution in the form of sedimentary rocks. Both Earth and Mars have a well-defined atmosphere, hydrosphere, cryosphere, and lithosphere. Interactions among these elements give rise to the flow of currents of air, liquid water, and ice, that in turn transport sediments from sites of weathering and erosion where they are formed, to sites of deposition where they are stored, to create a stratigraphic record of layered sediments and sedimentary rocks. This gives rise to the "source-to-sink" concept by which sedimentary systems on Earth have been characterized (Fig. 1). This unifying concept allows efficient comparison between planets. Our study of Mars has matured to the point where source-to-sink has found remarkable analogous application, and even Titan shows strong evidence for source-to-sink systems, albeit formed under very different conditions than either Earth or Mars. Venus, while recently resurfaced by volcanism and lacking a hydrosphere, also shows evidence for sediment transport in the form of surficial aeolian deposits. This provides clear evidence of the general validity of the approach (Fig. 2).

Time and history also are critically important cornerstones of the sedimentary record. Our understanding of the evolution of Earth's very ancient climate derives from detailed examination of the mineralogic, textural, and geochemical signatures preserved in the sedimentary rock record. Furthermore, Earth's sedimentary record attests to the formation and evolution of continents, plate tectonics, surface temperature, the composition of the atmosphere and

oceans, the evolution of life and the biogeochemical cycle of carbon, and the occurrence of extraordinary events in the history of climate — to name just a few examples (Fig. 3a). On Mars, we are beginning to uncover a similarly impressive list of evolutionary milestones, including billion-year-scale changes in aqueously formed mineral assemblages, the role of large impacts on surface evolution, river systems that once extended at almost hemispheric scales, and recognition of a rock cycle featuring deposition and erosion of vast sequences of strata (Fig. 3b).

The goals of this paper are to provide an overview of the fundamental aspects of source-to-sink systems on Earth, Mars, Venus, and Titan. Each planet can be discussed in terms of weathering and erosion, transport, and deposition — all key parts of source-to-sink systems. Although evidence of deposition and a stratigraphic record for Venus and Titan are very limited, both planets can be evaluated with reference to weathering, erosion, and sediment transport. We then close with a discussion of the history of deposition on these planets, and what information is embedded within these ancient records.

2. PLANETARY SOURCE-TO-SINK SYSTEMS

Weathering and erosion sculpt planetary landscapes and generate sediment, which is redistributed to alluvial plains, deltas, lakes, and ocean bottoms, to form diverse eolian landforms (Fig. 1). This transfer of sediment and solute mass from source to sink plays a key role in the cycling of elements, water, fractionation of biogeochemically important isotopes, and the formation of soils, groundwater reservoirs, masses of sediment, and even the composition of the atmosphere. The objective of source-to-sink studies is to identify and attempt to quantify the mass fluxes of sediments and solutes across planetary surfaces (e.g., *Allen,* 2008).

This framework creates a convenient starting point in which to understand the broader significance of weathering, erosion, transport, and deposition of sediments. Whether or not sediment is ever deposited ultimately depends on two factors: weathering and erosion to produce a *supply* of sediments, and the capacity of the flow to maintain the *transport* of those sediments (see below). The simplest approximation for sedimentary timescales (e.g., *Paola and Voller,* 2005) assumes the conservation of mass per unit area of the land surface, and the balance of sediment being transported vs. that being deposited is illustrated by the expression

$$\frac{d\eta}{dt} = -\frac{dq_s}{dx} - \sigma + \Omega \quad (1)$$

where η is the elevation of the bed of sediment, q_s is the flux of sediment (both solid and dissolved loads), σ the

TABLE 1. Sedimentologically useful parameters.

	Venus	Earth	Mars	Titan
Gravity	8.9 m s^{-2}	9.8 m s^{-2}	3.7 m s^{-2}	1.35 m s^{-2}
Mean surface temperature	735 K	288 K	214 K	93.6 K
Density of hydrosphere	N/A	1030 kg m^{-3}	N/A	445–662 kg m^{-3}
Submerged specific density	N/A	1.65	1.65 1.04 (viscous brines)	0.5–1.2 (water ice) up to 2 (organics)
Viscosity of hydrosphere (kinematic)	N/A	10^{-6} m^2 s^{-1}	10^{-6} m^2 s^{-1} (water flows) 4×10^{-5} m^2 s^{-1} (viscous brines)	10^{-7}–10^{-6} m^2 s^{-1}
Viscosity of atmosphere	33.4 μPa s	18.1 μPa s	10.8 μPa s	6.2 μPa s
Atmospheric density	71.92 kg m^{-3}	1.27 kg m^{-3}	0.027 kg m^{-3}	5.3 kg m^{-3}
Atmospheric composition				
Nitrogen (N_2)	3.5%	78.08%	2.7%	95%
Oxygen (O_2)	almost zero	20.95%	almost zero	zero
Carbon Dioxide (CO_2)	96.5%	0.035%	95.3%	zero
Water vapor (H_2O)	0.003%	~1%	0.03%	zero
Other gases	almost zero	almost zero	2% (mostly Ar)	5% (methane)
Composition of crust				
Exposed crust (SiO_2)	47%	66%	49%	~0%
Exposed crust dominant material	Plagioclase, pyroxene, olivine	Quartz, plagioclase, K-feldspar	Plagioclase, pyroxene, olivine	Water ice and clathrate hydrate overlain by organic veneer
Dune material	Basalt	Quartz	Basalt	Organics (lower density)

Data sources: *Nesbitt and Young* (1984), *Surkov et al.* (1984), *Yung et al.* (1984), *Tobie et al.* (2006), *McLennnan and Grotzinger* (2008), *Taylor and McLennan* (2009), *Lorenz et al.* (2010), *Tosca et al.* (2011), *Choukroun and Sotin* (2012).

local rate of surface subsidence or uplift (negative) due to tectonics, and Ω is the net accumulation rate of sediment from the atmosphere (e.g., settling of photolysis particles on Titan). In this one-dimensional formulation x is taken as the down-current direction and sediment-bed porosity is neglected. In the absence of tectonic uplift or subsidence, as is likely the case on Mars, Titan, and Venus, and in the absence of atmospheric deposition (precipitation of solids) as is likely the case on Earth, Mars, and Venus (excluding regions where ice deposits form), equation (1) simplifies to

$$\frac{d\eta}{dt} = -\frac{dq_s}{dx} \tag{2}$$

The relation states that bed elevation increases proportionally to the amount of sediment that drops out of transport, and conversely decreases proportionally to the amount of sediment that becomes entrained by the flow. In sediment source areas, sediment flux is typically limited by the conversion of rock to sediment (i.e., a sediment supply limited landscape); these landscapes tend to be net erosional and q_s is set by the erosional processes at work including weathering, river incision into bedrock, and abrasion by wind, for example. In sediment bypass and depositional areas, sediment supply is typically abundant, and therefore q_s is set by the ability of a flow to transport sediment [i.e., a transport limited landscape (*Howard et al.,* 1994)]. For these cases, sediment flux and therefore deposition rate (equation (2)) is governed by the flow dynamics alone; in effect, wherever the current slows — usually due to a divergence in the flux of fluid — net sedimentation will result. On the other hand, when the current velocity increases, net erosion will result.

In one other simplification, in many cases it can be assumed that flows of liquid across planetary surfaces will move downhill, in response to gravity, and flows of air will move in response to regional gradients in atmospheric pressure. The influence of tides and geostrophic flows associated with Earth's global ocean are a very important process that we will ignore in this paper. The simplification results in the formulation of a straightforward constitutive law for sediment transport

$$q_s = -K\frac{d\eta}{dx} \tag{3}$$

where K is a transport coefficient that takes into account all the detailed mechanics of sediment transport (see below), and may not always be independent of x as assumed here. This transport law states that sediment transport is proportional to slope and is based on theoretical, experimental, and empirical analyses of downslope transport by creep, overland flow, and channel flow processes.

Substituting equation (3) into equation (2) yields

$$\frac{\partial\eta}{\partial t} = K\frac{\partial^2\eta}{\partial x^2} \tag{4}$$

which states that topographic evolution through sediment transport follows a linear diffusive process. This simple model of erosion and sedimentation can effectively account for a vast range of source-to-sink systems on Earth (e.g., *Kenyon and Turcotte,* 1985; *Flemings and Grotzinger,* 1996; *Paola,* 2000), and likely on other planets as well where gravity results in net downslope transport of liquid and

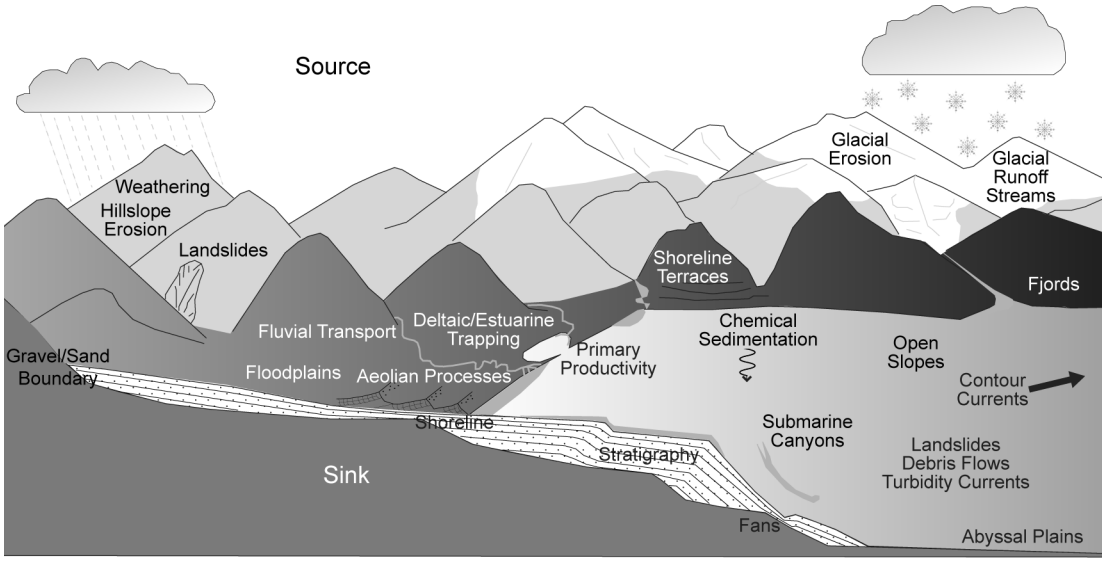

Fig. 1. Surface processes on Earth give rise to sediments in source areas that are transported to sites of deposition, or sinks. This "source-to-sink" concept is applicable, with modifications, to Mars and Titan.

sediment. Figure 4a shows a simple model of an alluvial fan based on a two-dimensional diffusion model of sediment transport (STRATA) (see *Flemings and Grotzinger,* 1996). In this example the source (flux) of sediment is provided through the lefthand boundary and redistribution of that flux is regulated by the topography of the fan as it builds through time. Over time the profile adjusts so that the time lines of the model output converge to indicate the flux into the leftmost cell is mostly balanced by the flow out of the rightmost cell. The morphology of the modeled fan surface is close to equilibrium. One must envisage the righthand boundary passing, in reality, from the fan into an adjacent geomorphic feature such as a playa lake.

Such a simple system as shown in Fig. 4a illustrates the source-to-sink concept. We can implement a simple perturbation, taken to simulate climate change — say an increase in water flux through enhanced precipitation — that results in an increase in the flux of sediment to the fan (Fig. 4b). The system response is apparent and this forward model of the history of deposition can be used to illustrate how the inverse problem — recovery of climate history — could be addressed using the record of sedimentation.

We now turn to more detailed descriptions of the components of planetary source-to-sink systems. Sediment production by weathering and erosion is first described, and then the discussion moves on to sediment transport and deposition, and we end with a discussion of the planetary stratigraphic record (sedimentary history), with emphasis on events that represent past changes in climate.

3. WEATHERING

The weathering process initiates changes, separation, and redistribution of rock fragments, minerals, and chemical elements within the surficial environment of a planet and accordingly is the starting place for the source-to-sink sedimentary paradigm. Although classical weathering takes place mainly within soil profiles, the transport of sediment from the initial source to the final depositional basin may involve many intervening short-term stages of deposition and reerosion during which both physical and chemical weathering processes act further on the sedimentary material (*Johnsson and Meade,* 1990). For longer timescales (>~10^5–10^6 yr), it is worth remembering that on Earth approximately 70% of sediment on average is derived from weathering and erosion of preexisting sedimentary rocks, and accordingly the influences of weathering on mineralogy and geochemistry can accumulate over several sedimentary cycles (*Veizer and Mackenzie,* 2003). A key

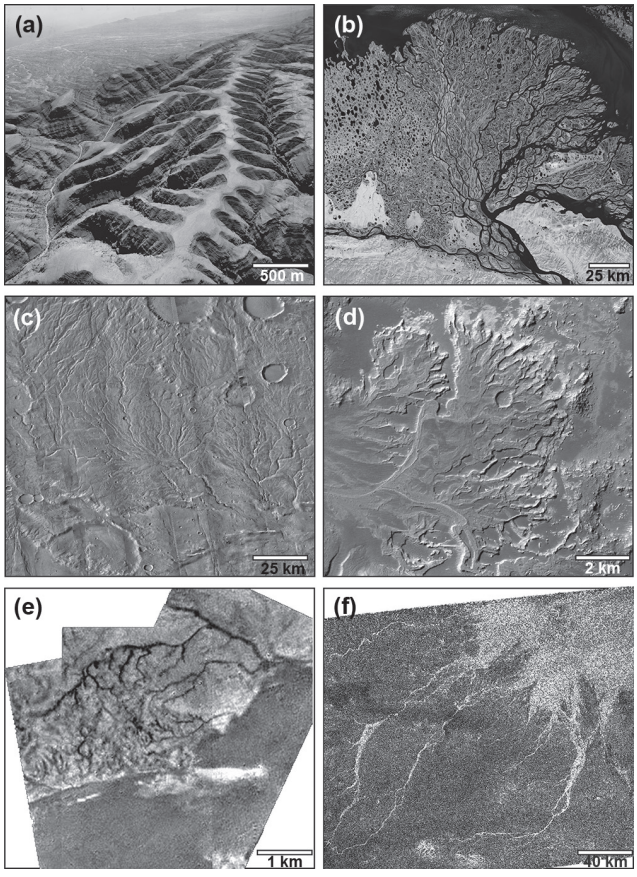

Fig. 2. Source-to-sink systems on Earth, Mars, and Titan. **(a)** Source region on Earth, where surface runoff results in bedrock channel incision, and formation of stream networks, Mirbat escarpment, southern Oman. Oblique aerial photograph, Petroleum Development Oman. **(b)** River delta represents a sediment sink where divergence in the flux at the edge of the continent results in sediment deposition. Lena river delta, northern Siberia. Landsat 7 image, NASA. **(c)** Source region on Mars at Solis Planum (–41.7 N, 266.8 E) with well-developed branched stream network developed in bedrock. It has been inferred that such networks are consistent with ancient atmospheric precipitation of water. CTX images, from east to west: P21_009263_1379_XN_42S091W, B05_011531_1378_XI_42S091W , P07_003633_1378_XI_42S092W, B04_011386_1388_XI_41S092W, P04_002710_1375_XI_42S092W, P07_003699_1373_XI_42S093W, P22_009540_1376_XN_42S093W, B02_010318_1381_XI_41S094W, P08_004121_1379_XI_42S094W, B19_016898_1377_XN_42S094W, P10_005110_1383_XI_41S095W. **(d)** Eberswalde delta represents a local sediment sink on Mars within an impact crater. Flow from a broad region surrounding the crater gathered water and sediment that entered the impact basin as a single channel stream; divergence of this flux at the entry point, in what was inferred to have been a lake, resulted in creation of the delta. CTX image B18_016777_1580_XN_22S034W. **(e)** Source region at Huygens probe landing area on Titan (10°S, 192°W). The dendritic network drains into an alluvial plain that is strewn with decimeter-scale water-ice cobbles. Near-infrared (660–1000 nm) mosaic of frames from the Huygens Descent Imager and Spectral Radiometer (DISR). **(f)** Potential alluvial fan at Elvigar Flumina (19.3°N,78.5°E) on Titan, which may represent a local sediment sink. Ku-band Synthetic Aperture Radar (SAR) image acquired by the Cassini spacecraft on February 15, 2005.

issue in interpreting the history of weathering in terms of source-to-sink processes is distinguishing the *intensity* of weathering (controlled largely by climate) and the *duration* of weathering [controlled largely by physical characteristics such as slope, relief, mass wasting rates (*Johnsson,* 1993)]. This issue becomes especially relevant on Mars and other planetary surfaces where age and duration of most processes are very poorly constrained.

On Earth, the intensity of weathering provides a direct link to climate through the carbon biogeochemical cycle, for example, by consuming CO_2 from the atmosphere during weathering reactions and transporting dissolved carbon (mainly as bicarbonate) to the oceans where it may be precipitated and stored in carbonate rocks. There is some relationship between weathering rates and surface temperatures, but the details are complex (e.g., *West et al.,* 2005). On Mars and Venus, any link between weathering and climate may also be strongly influenced by an analogous sulfur cycle (see further discussion below). In addition, the mineralogical and geochemical (including isotopic) composition of sediments

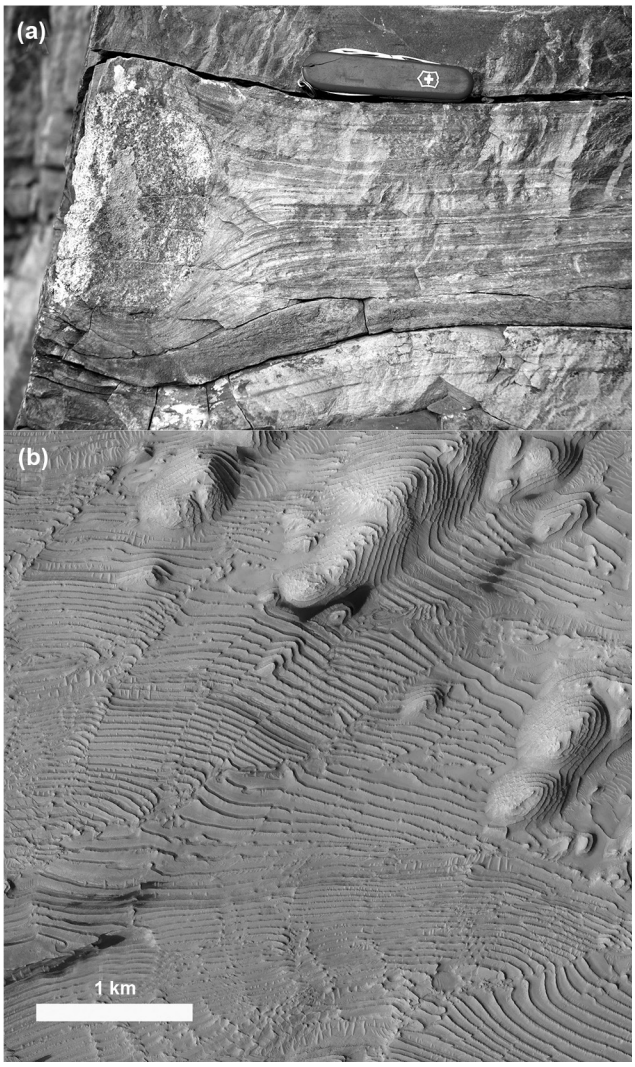

Fig. 3. Inferred records of climate preserved in the very ancient stratigraphic records of Earth and Mars. **(a)** Large stone (on left) dropped from melting glacier, and termed a "dropstone," pierces and then is overlain by fresh sediment in ~635-m.y.-old marine deposits, Sultanate of Oman. Penknife is 7 cm long. **(b)** Highly rhythmic strata are interpreted to record obliquity changes on Mars over 2 b.y. ago. Danielson crater, Arabia Terra region, HiRISE image PSP_002733_1800.

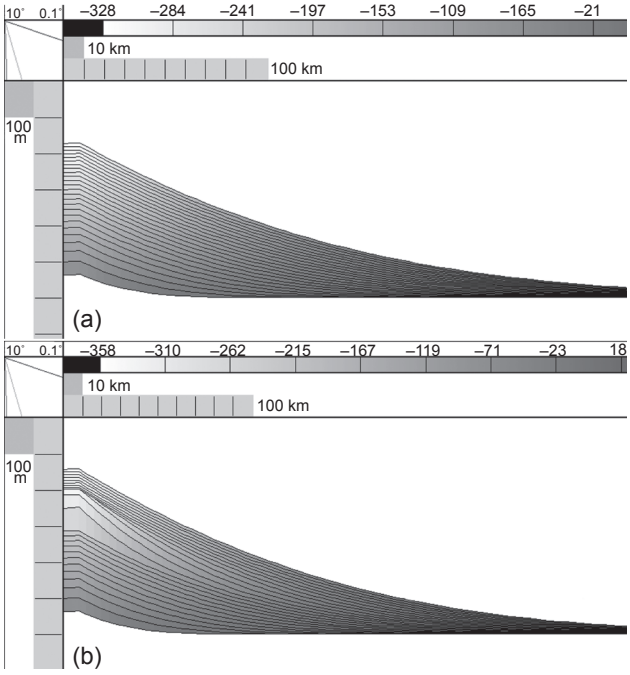

Fig. 4. STRATA is a forward model of sedimentation based on solving simple sediment transport (diffusion) equation for different initial conditions. Output displays cross-sections through synthetic alluvial fan deposits with black lines marking the geomorphic evolution of the fan at constant time values. Scale bars shown, vertical exaggeration indicated by slopes in upper lefthand corners of plots, and gray scale is water depth — with negative values corresponding to elevation of alluvial above datum. **(a)** Sediment is supplied from the lefthand boundary with a flux of 50 m^2/y. With time the fan acquires a steady-state profile at which point the flux of sediment in from the left boundary (into the fan) is equal to the flux out of the right boundary (out of the fan). **(b)** All parameters as in **(a);** however, the flux is abruptly changed from 50 to 100 m^2/y about halfway through the run. This simulates a change in climate (e.g., from relatively dry to wetter), which in turns stimulates increased sediment production. The profile of the fan changes (steepens) in response but then relaxes as the system once again approaches steady state. This is important because it means that, on the basis of geometry alone, ancient strata can be used to infer the very ancient climate of past planetary history. Such an approach has worked well on Earth (*Dorn,* 2009) and should be applicable to Mars and perhaps Titan.

being deposited at any given time provides a proxy for the penecontemporaneous climate and so a record of climate change is preserved within the stratigraphic record.

3.1. A Planetary Perspective on Weathering

Weathering conventionally is subdivided into chemical, physical (or mechanical), and biological processes (*Brantley et al.,* 2007; *Brantley and Lebedeva,* 2011), but in reality these boundaries are largely artificial and in detail these processes act in a highly synergistic manner. For example, salts may be chemically deposited within rock fractures that in turn undergo repeated thermal expansion during diurnal cycles, thus promoting physical disintegration. Impact processes result in the generation of large amounts of mechanically generated particles, thus providing great surface area upon which chemical reactions may take place. In a uniquely terrestrial example, root systems of plants serve to physically disrupt invaded rocks, thus promoting physical weathering, but also influence chemical gradients within soils that can greatly facilitate chemical weathering reactions.

The sedimentary cycles of atmosphere-bearing rocky planetary bodies, whether the familiar terrestrial cycle — intimately related to plate tectonics and biological activity — or a less-familiar surface such as Venus, weathering mostly accomplishes two fundamental roles. Chemical weathering begins the process of reequilibrating surface rocks and minerals, formed at relatively high pressures and temperatures and under differing volatile conditions (e.g., f_{O_2}, f_{CO_2}, f_{SO_2}, a_{H_2O}), with planetary surface conditions that typically are at lower temperature and pressure and with different but highly variable aqueous and volatile conditions. As part of this process, when a dynamic hydrological cycle also exists, constituents from the primary rocks and minerals may be liberated and dissolved into aqueous solutions (or held as colloids) to be chemically deposited later by various processes (evaporation, biological activity, diagenesis, etc.). In more exotic cases rock-atmosphere-hydrosphere interaction may be impeded by icy crusts that in turn may interact with any available near-surface fluids, which in the case of Titan is methane and ethane, and/or undergo "sublimation weathering" in cases where temperatures are too low for liquid water (*Melosh,* 2011). Weathering also promotes mechanical breakdown of rocks and minerals (and in the case of Titan, ices and solid organics), typically facilitated by chemical (and in the case of Earth, biological) processes, into sedimentary particles of widely varying size and composition that can then be physically transported from their sources and deposited into sedimentary basins and also become the agents for further physical weathering and erosion.

We are concerned here with sedimentation on Earth, Mars, Titan, and Venus where substantial atmospheres exist and sedimentary records have been established to varying degrees. However, weathering in some form takes place on all planetary surfaces, even on airless bodies (*Melosh,* 2011). For example, asteroidal parent bodies from which water-rich carbonaceous chondrites (CI, CM, CR, CV, and CH types) were derived are characterized by varying degrees of low-temperature, largely isochemical aqueous alteration resulting in a wide variety of secondary phases (e.g., phyllosilicates, carbonates, sulfates). On airless bodies such as the Moon, Mercury, and asteroids, ionizing particle radiation from solar winds and cosmic rays and meteorite, micrometeorite, and cosmic dust bombardment result in a set of diverse processes collectively termed space weathering. The effects of space weathering include formation of glasses and agglutinates in planetary regolith, implantation of gases, damage to crystal structures, reduction of ferrous iron (e.g., in olivine) to nanophase Fe^0, and general darkening/reddening of planetary surfaces (*Gaffey,* 2010). Although space weathering affects only the outermost few nanometers of exposed surfaces, impact gardening redistributes and effectively sequesters affected material into the deeper regolith.

Terrestrial chemical weathering is controlled by the carbon cycle in which weak carbon-based acids [i.e., carbonic (pK_a ~ +6.5) and organic acids (pK_a mostly >+2)] dominate chemical weathering processes under mildly acidic to circumneutral pH (~5–8) conditions (*Berner,* 1995). Although sulfur forms important volcanic gases, the sulfur cycle plays a lesser role in global weathering because sulfur is readily transferred through the ocean into the sedimentary rock record (facilitated by microorganisms, for example, through the process of bacterial sulfate reduction) and further recycled through the mantle by plate tectonics (*Canfield,* 2004). Earth's atmosphere contains only sub-parts per billion levels of total sulfur as various gaseous compounds. However, from a planetary perspective, sulfur cycles rather than carbon cycles may be more influential in controlling weathering processes. In the absence of plate tectonics and large water masses, sulfur-bearing minerals accumulate on the surface of planets (or as sulfur-bearing atmospheric compounds), as witnessed on the surfaces of Mars (*King and McLennan,* 2010) and Mercury (*Nittler et al.,* 2011) and in the atmosphere of Venus where the concentration of SO_2 in the 9.7 MPa atmosphere is about 150 ppmv (*Johnson and Fegley,* 2002). Since sulfur forms strong acids (e.g., sulfuric acid; pK_a ~ –3), oxidative weathering processes dominated by a sulfur cycle are more likely to take place under much lower pH conditions (*Johnson and Fegley,* 2002; *Halevy et al.,* 2007; *McLennan,* 2012).

In the sections below, we will discuss some major influences on physical and chemical weathering on Earth, Mars, Venus, and Titan. From a broader planetary perspective, another key factor that must also be kept in mind is the role of impacts in producing sedimentary particles. Many planetary surfaces, including large regions of Mars, Mercury, and the Moon, are very ancient (≥3.8 Ga) and accordingly are strongly influenced by impact processes on many scales, which serve an important role in physically fracturing and disrupting rocks to expose large surface areas. Impacts also serve to vertically mix surface regolith through the process of impact gardening, thus influencing the overall weathering process (*Melosh,* 2011). On airless bodies, impact-induced regolith remains locally distributed,

whereas on planetary bodies with atmospheres and hydrospheres, such as those considered here, impact-produced debris may be redistributed over large regions by aeolian and aqueous processes (*Grotzinger et al.,* 2011). Weathering acts to further facilitate the production of particles that form sediment. These sediment particles can cause erosion by acting as tools for abrasion.

3.2. Terrestrial Weathering

On Earth, weathering takes place within the so-called "critical zone," the near-surface region of the planet, between the deepest groundwater and the outer extent of vegetation, where interacting geological, chemical, physical, and biological activity supports life.

3.2.1. Chemical weathering. Chemical weathering includes various processes involving the interaction of aqueous solutions, mostly shallow groundwater, with rocks at and near the Earth's surface (Fig. 5). The overall result is (1) transformation of primary igneous-metamorphic rocks and minerals into a suite of secondary minerals that are more stable under ambient surficial conditions (e.g., clays and insoluble oxides); (2) transfer into aqueous solution of soluble components (e.g., Ca^{2+}, Mg^{2+}, K^{+}, Na^{+}, HCO_3^{-}, SO_4^{2-}, Cl^{-}) that may be redistributed within the weathering profile or carried out of the soil system to be deposited elsewhere; and (3) weakening and disruption of the critical zone, contributing to episodes of mass wasting and exposure of fresh rock to weathering solutions. Numerous processes are involved, including hydrolysis, dissolution, oxidation, hydration-dehydration, carbonation, ion exchange, and chelation. Of these reactions, hydrolysis is the most important volumetrically for generating the terrestrial sedimentary rock record. Hydrolysis involves the movement of free H^{+} (or H_3O^{+}) in aqueous solutions into rocks and minerals, first along fractures and mineral/grain boundaries and then by diffusion into crystal structures. Protons release and/or replace other ions in mineral structures to either dissolve the primary mineral, e.g., olivine dissolution

$$Mg_2SiO_{4(\text{forsterite})} + 4H^{+} \Leftrightarrow 2Mg^{2+} + H_4SiO_{4(\text{orthosilicic acid})} \quad (5)$$

or alter the primary mineral to a more thermodynamically stable mineral, e.g., anorthite ⇒ kaolinite (Fig. 5)

$$CaAl_2Si_2O_{8(\text{anorthite})} + 2H^{+} + H_2O \Leftrightarrow Al_2Si_2O_5(OH)_{4(\text{kaolinite})} + Ca^{2+} \quad (6)$$

An important development in quantitatively understanding the chemical and mineralogical changes associated with weathering processes is the development of the chemical index of alteration (CIA) concepts (e.g., *Nesbitt and Young,* 1984; *Nesbitt and Wilson,* 1992; *Nesbitt and Markovics,* 1997; *Nesbitt,* 2003). This can be seen on the "feldspar ternary" that plots mole proportions of Al_2O_3–($CaO^* + Na_2O$)–K_2O, or A-CN-K (Fig. 6a), where CaO* represents the calcium in silcate minerals and is thus corrected for carbonates and phosphates. Such a diagram captures most of the major-element (and thus mineralogical) changes observed in the weathering of granitic (sensu lato) rocks. The CIA scale [$CIA = 100 \times Al_2O_3/(Al_2O_3 + CaO^* + Na_2O + K_2O)$] is shown on the left of Fig. 6a. Typical weathering trends for different igneous rock compositions, constrained from thermodynamic-kinetic studies of feldspar and glass alteration (e.g., *Nesbitt and Young,* 1984) and field studies of weathering profiles, are also shown and illustrate the dissolution of mafic minerals and reaction of plagioclase to clay followed by the reaction of K-feldspar to clay, leading in the most extreme examples to highly aluminous clay-rich soils.

The susceptibility of igneous minerals to weathering processes is well known to approximate the reverse of the Bowen's igneous reaction series (*Goldich,* 1938). However, a more quantitative expression of this relationship can be seen from the Gibbs free energies of various weathering reactions expressed on a per atom basis (*Curtis,* 1976) (Table 2). Thus mafic minerals such as olivine, pyroxene, and Ca-plagioclase are more readily dissolved and altered than are minerals from more evolved igneous settings, such

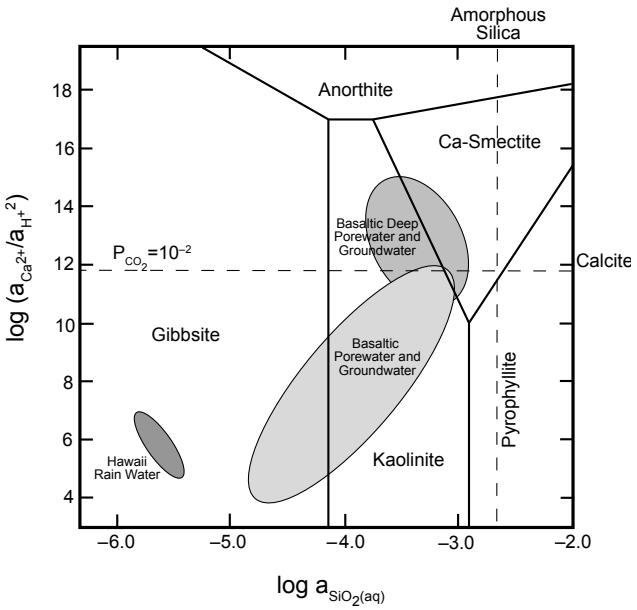

Fig. 5. Mineral stability diagram plotting $a_{Ca^{2+}}/a_{H^+}^2$ vs. $a_{SiO_2(aq)}$ (where a is activity) showing the stability relationships among pure anorthite and various clay minerals at standard temperature and pressure (25°C; 1 bar). Dashed lines are solubility limits for calcite (P_{CO_2} = 10^{-2} atm) and amorphous silica. Also shown are typical compositions for Hawaiian rainwater and groundwaters taken from different depths in selected basaltic terrains. Adapted from *Nesbitt and Wilson* (1992). This diagram illustrates the fundamental instability of a common basaltic igneous mineral in the presence of near-surface waters.

as K-feldspar. In detail many other factors, such as pH and other ion activities, can also affect mineral stabilities.

Much work has been carried out to evaluate the kinetics of weathering reactions and timescales for the formation of weathering profiles (see numerous reviews in *White and Brantley,* 1995; *Oelkers and Schott,* 2009). A long-standing issue is the lack of agreement between chemical weathering rates determined in the field compared to those determined in the laboratory, the former typically being several orders of magnitude slower. The major sources of this discrepancy have to do with the changing character of mineral surfaces (e.g., lowering of reactive surface areas as heterogeneities diminish; development of physical barriers due to leaching and/or deposition of precipitates) and changes in evolving aqueous fluids (e.g., changing saturation states) as natural weathering proceeds. It is important to keep the differences between natural and laboratory rates in mind when considering weathering from a planetary perspective, since on most planets, detailed field studies are either limited (e.g., Mars) or unavailable (e.g., Venus, Titan) and experiments are heavily relied on to gain insight.

3.2.2. The importance of basaltic weathering. From a planetary perspective, many studies of chemical weathering on Earth are not particularly informative. Terrestrial weathering takes place mostly on igneous/metamorphic rocks of the upper continental crust or on sedimentary rocks ultimately derived from the upper continental crust (*Taylor and McLennan,* 1985). The exposed upper continental crust of Earth approximates to a granodioritic composition on average and the "tertiary" continental crust is unique within the solar system (*Taylor and McLennan,* 2009). Instead, planetary surfaces are predominantly characterized by "primary" and "secondary" crusts composed of mafic and ultramafic rocks. This can be seen from Table 3, which tabulates estimates of the chemical composition (and mineralogy) of the terrestrial upper continental crust and martian exposed crust. There is no reliable estimate for the average exposed venusian crust, but remote sensing and available surface analyses (Table 3) also indicate a basaltic composition (*Taylor and McLennan,* 2009).

Accordingly, terrestrial studies that focus on the weathering of basaltic rocks (Fig. 6b) and minerals are far more relevant (e.g., *Nesbitt and Wilson,* 1992; *Brantley and Chen,* 1995; *Louvat and Allegre,* 1997; *Stefannsson and Gislason,* 2001; *Navarre-Sitchler and Brantley,* 2007). Primary mineralogy in such weathering systems is dominated by olivine, pyroxenes, plagioclase, and Fe-Ti-oxides (*McLennan and Grotzinger,* 2008; *Taylor et al.,* 2008). Accordingly, the "mafics ternary" plotting Al_2O_3–(CaO* + Na_2O + K_2O)–(FeO_T + MgO), or A-CNK-FM, better captures the geochemical variation. During basaltic weathering the relative importance of alteration to clays, compared to primary mineral dissolution, is considerably less than for weathering of granitic compositions (Table 2).

3.2.3. Physical weathering. Most physical weathering processes involve differential volume changes whereby

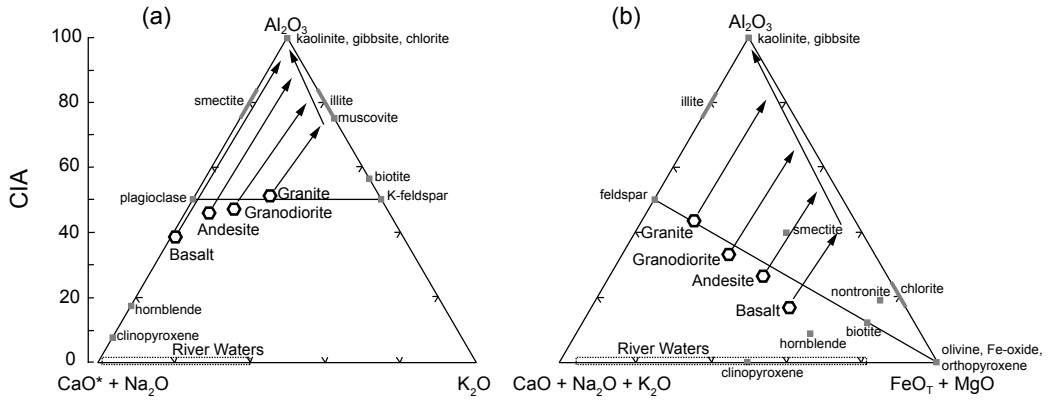

Fig. 6. Ternary diagrams plotting molar proportions **(a)** Al_2O_3–(CaO* + Na_2O)–K_2O, or A-CN-K, and **(b)** Al_2O_3–(CaO* + Na_2O + K_2O)–(FeO_T + MgO), or A-CNK-FM, illustrating weathering trends in terrestrial settings (adapted from *Nesbitt and Young,* 1984; *Nesbitt and Wilson,* 1992). CaO* refers to calcium in the silicate components only (i.e., corrected for carbonates and phosphates). The CIA scale is plotted on the left side of the A-CN-K diagram. Plotted are selected igneous and sedimentary minerals, average compositions of major igneous rock types and the range for most natural waters. The thin horizontal line on the A-CN-K diagram (connecting plagioclase and K-feldspar) and the thin diagonal line on the A-CNK-FM diagram (connecting feldspar to FM apex) effectively separate the lower parts of the diagrams dominated by primary igneous minerals (unweathered) from the upper parts dominated by clays (weathered). The arrows schematically indicate general trends for increasing degrees of weathering for various rock types, based on field studies of weathering profiles and thermodynamic/kinetic modeling.

TABLE 2. Some common simplified weathering reactions with their Gibb's free energy of reaction at standard temperature (25°C) and pressure (1 bar) (after *Curtis,* 1976).

		ΔGr^0 (Kcal/mole)	ΔGr^0 (Kcal/gram atom)
Sulfide			
Pyrite oxidation	$2FeS_{2(s)} + 4H_2O_{(l)} + 7.5O_{2(g)} \Leftrightarrow Fe_2O_{3(s)} + 4SO_4^{2-}{}_{(aq)} + 8H^+{}_{(aq)}$	–583.5	–17.68
Olivine			
Fayalite ⇒ hematite	$Fe_2SiO_{4(s)} + 0.5O_{2(g)} \Leftrightarrow Fe_2O_{3(s)} + SiO_{2(s)}$	–52.7	–6.58
Forsterite dissolution	$Mg_2SiO_{4(s)} + 4H^+{}_{(aq)} \Leftrightarrow 2Mg^{2+}{}_{(aq)} + 2H_2O_{(l)} + SiO_{2(s)}$	–44.0	–4.00
Pyroxene			
Enstatite dissolution	$MgSiO_{3(s)} + 2H^+{}_{(aq)} \Leftrightarrow Mg^{2+}{}_{(aq)} + H_2O_{(l)} + SiO_{2(s)}$	–20.9	–2.98
Diopside dissolution	$CaMg(SiO_3)_{2(s)} + 4H^+{}_{(aq)} \Leftrightarrow Ca^{2+}{}_{(aq)} + Mg^{2+}{}_{(aq)} + 2H_2O_{(l)} + 2SiO_{2(s)}$	–38.1	–2.72
Amphibole			
Anthopyllite dissolution	$Mg_7Si_8O_{22}(OH)_{2(s)} + 14H^+{}_{(aq)} \Leftrightarrow 7Mg^{2+}{}_{(aq)} + 8H_2O_{(l)} + 8SiO_{2(s)}$	–137.2	–2.49
Tremolite dissolution	$Ca_2Mg_5Si_8O_{22}(OH)_{2(s)} + 14H^+{}_{(aq)} \Leftrightarrow 2Ca^{2+}{}_{(aq)} + 5Mg^{2+}{}_{(aq)} + 8H_2O_{(l)} + 8SiO_{2(s)}$	–123.2	–2.24
Feldspar			
Anorthite ⇒ kaolinite	$CaAl_2Si_2O_{8(s)} + 2H^+{}_{(aq)} + H_2O_{(l)} \Leftrightarrow Al_2Si_2O_5(OH)_{4(s)} + Ca^{2+}{}_{(aq)}$	–23.9	–1.32
Albite ⇒ kaolinite	$2NaAlSi_3O_{8(s)} + 2H^+{}_{(aq)} + H_2O_{(l)} \Leftrightarrow Al_2Si_2O_5(OH)_{4(s)} + 2Na^+{}_{(aq)} + 4SiO_{2(s)}$	–23.1	–0.75
Microcline ⇒ kaolinite	$2KAlSi_3O_{8(s)} + 2H^+{}_{(aq)} + H_2O_{(l)} \Leftrightarrow Al_2Si_2O_5(OH)_{4(s)} + 2K^+{}_{(aq)} + 4SiO_{2(s)}$	–15.9	–0.51

TABLE 3. Chemical and mineralogical comparison of the terrestrial upper continental crust, martian upper crust, and available analyses from the Venus surface.

	Earth	Mars	Venus		
	Upper Crust	Upper Crust	Vega 2	Venera 13	Venera 14
SiO_2	65.9	49.3	45.6	45.1	48.7
TiO_2	0.65	0.98	0.2	1.59	1.25
Al_2O_3	15.2	10.5	16.0	15.8	17.9
FeO_T*	4.52	18.2	7.7	9.3	8.8
MnO	0.08	0.36	0.14	0.2	0.16
MgO	2.21	9.06	11.5	11.4	8.1
CaO	4.20	6.92	7.5	7.1	10.3
Na_2O	3.90	2.97	(2.0)	(2.0)	(2.4)
K_2O	3.36	0.45	0.48	4.0	0.2
P_2O_5	0.16	0.90	—	—	—
Other	—	—	5.0	1.9	1.3
Sum	100.2	99.6	96.1	98.4	99.1
Olivine	—	17	19	29	10
Pyroxene	1	22	22	11	27
Fe-Ti oxides	1	10	<1	3	2
Glass	13	21	—	—	—
Plagioclase	35	29	55	24	59
K-feldspar	11	—	3	25	1
Sheet silicates	14	—	—	—	—
Quartz	20	—	—	—	—
Nepheline	—	—	—	9	
Other	4	—	—	—	—

*Total iron as FeO_T.

Chemical compositions in weight percent. Data sources: Earth upper crust chemistry and mineralogy from *Nesbitt and Young* (1984) and *Taylor and McLennan* (2009); martian upper crust chemistry and mineralogy from *McLennan and Grotzinger* (2008) and *Taylor and McLennan* (2009); Venus chemical analyses from *Surkov et al.* (1984, 1986, 1987) (note that Na_2O was not analyzed and values are estimates from Surkov et al. and that "Other" includes SO_3 and Cl), and Venus mineralogy are CIPW norms based on volatile-free compositions assuming all Fe as FeO.

shear stresses, on a variety of scales ranging from crystals/grains to large outcrops, cause expansion/contraction that in turn destabilizes some part of a rock mass. *Melosh* (2011) recently reviewed physical weathering processes on planetary surfaces, including Earth [his terminology and organization differ somewhat from terrestrially oriented geomorphology texts (e.g., *Easterbrook,* 1999)]. The processes identified include (*Melosh,* 2011)

1. Stress corrosion cracking involving the propagation of fractures assisted by chemically reactive fluids (providing an environmental and kinetic framework) and influencing formation of fractures on a broad range of scales from microscopic cracks on mineral surfaces through to larger scale vertical joints.

2. Sheeting and exfoliation joints, which are near-surface, subhorizontal features formed as a result of vertical stress release giving rise to upward rock expansion and fracture growth due to compressive stresses parallel to the planetary surface.

3. Spheroidal weathering, which results from chemical weathering where fluids percolate along preexisting joint-bounded fractures leading to corestones within soils (e.g., Fig. 7) and to free-standing monoliths, called tors, that are preserved on some mass-wasted weathered surfaces.

4. Frost shattering resulting from growth of ice crystals in fractures fed by thin films of fluid (water in the case of Earth) that have significantly depressed freezing temperatures. On Earth such processes can exert pressures of ~10 MPa. Frost shattering currently is probably of negligible importance on Mars (atmospheric pressure below triple point of water), Venus (always above melting temperature), or Titan (where the liquid is a hydrocarbon; see section 3.5).

5. Salt weathering resulting from crystallization of dissolved salts (typically halite on Earth) within rock fractures and is thus a similar process to frost shattering. Crystallization pressures of common evaporite minerals are in the range of ~10–55 MPa.

6. Rock disintegration in response to volume changes that typically result from various processes (e.g., mineral reactions, clay swelling/shrinking). On Earth this process generates quartz sand grains, but its role in producing sand-sized particles on planets with basaltic surfaces is less well understood. For example, on Mars olivine sands appear fairly common and may form by rock disintegration leaving behind the relatively hard olivine. Plagioclase is also a common basaltic phenocryst mineral, is more resistant to chemical weathering than olivine, but has not yet been identified as an especially abundant sand grain. On the other hand, plagioclase cleavage probably makes it more susceptible to physical breakdown than olivine.

7. Insolation weathering resulting from thermal stresses generated from diurnal temperature changes. The lack of evidence for this process on the Moon, where temperature changes are extreme, suggests that the process also requires aqueous activity.

Additional erosional processes are also important in understanding physical weathering. As weathering profiles develop on slopes from chemical-physical-biological activity they inevitably become gravitationally unstable and are transported downslope by soil creep and mass wasting. Transport of particles, by either aeolian or fluvial processes, further lead to saltation abrasion of substrate surfaces by bouncing particles, and highly energetic transport (e.g., rock falls) results in rock shattering. During glacial transport large amounts of fine-grained sediment are produced by physical grinding, and rock plucking is also a common process influencing the weathering surface over which glaciers travel.

What is the relative role of chemical vs. physical weathering processes in the formation of sediment? By comparing the particulate and dissolved loads within rivers, *Millot et al.* (2002) derived an empirical relationship between chemical (R_{Chem}) and physical (R_{Phys}) weathering rates (in tons/km^2/yr)

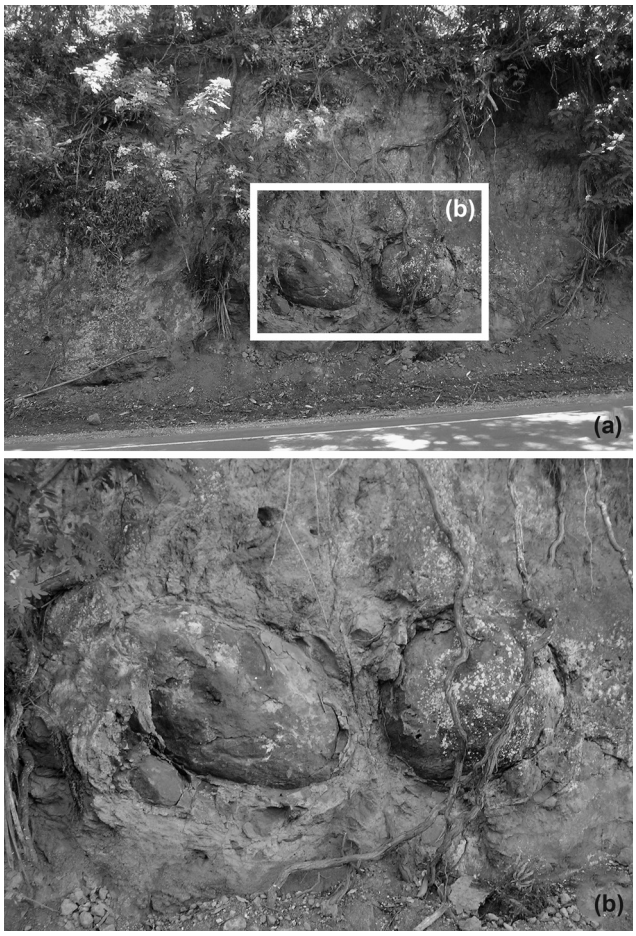

Fig. 7. **(a)** Photograph showing corestone weathering features in a soil horizon formed on the Kohala volcano on the north side of Hawai'i Island. **(b)** Close up of corestones showing the exfoliating surface. The circular corestone on the right is approximately 1 m in diameter.

$$R_{Chem} = 0.39 \times \left(R_{phys} \right)^{0.66} \quad (7)$$

that appears to apply to sediments derived from both granitic and basaltic terranes. This relationship is broadly consistent with that determined from an evaluation of chemical/physical denudation rates in soils (*Anderson et al.,* 2007).

3.2.4. Biological processes. Biological activity is well known to strongly influence physical weathering (e.g., root growth, bioturbation of soils), but a more recent development is recognition of the importance of biological activity in also promoting chemical weathering related to chemical gradients and microenvironments (e.g., in pore space) set up both by macroscopic organisms (e.g., root systems) and microbial activity (*Nesbitt,* 1997; *Berner et al.,* 2004; *Chorover et al.,* 2007; *Amundson et al.,* 2007). On the other hand, from a planetary perspective, it is not yet possible to evaluate the significance of such processes beyond Earth.

3.3. Weathering on Mars

3.3.1. Chemical processes. The red color of Mars has long sent the message that some form of secondary (oxidative) weathering affected the surface and this was confirmed by early remote sensing that indicated the presence of ferric iron (*Burns,* 1993). Evidence for the occurrence of aqueous alteration first came from *in situ* chemical measurements of soils that have high sulfur and chlorine abundances and can be modeled to represent mixtures of silicate minerals and sulfate/chloride salts using mass balance calculations (e.g., *Clark et al.,* 1976; *Clark, 1993; Foley et al.,* 2008; *Haskin et al.,* 2005; *Ming et al.,* 2006; *Hurowitz and McLennan,* 2007; *McLennan and Grotzinger,* 2008; *Hecht et al.,* 2009; *McLennan,* 2012). Recent acquisition of Mössbauer spectrometry, thermal infrared spectroscopy, and microscopic imaging of textures allow for considerable refinement of such models. For example, *McSween et al.* (2010) (see also *McGlynn et al.,* 2012) modeled Meridiani and Gusev soils as mixtures of ~75 ± 5% unaltered igneous components (plagioclase, pyroxene, olivine, oxides, phosphates) and ~25 ± 5% of a secondary alteration assemblage (sulfates, silica, clays, secondary oxides, chlorides). These values provide possible insight into the overall scale of chemical alteration that has affected the martian surface.

Many lines of evidence indicate that Mars has experienced a long-lived chemically dynamic sedimentary rock cycle (see reviews in *McLennan and Grotzinger,* 2008; *Grotzinger et al.,* 2011; *McLennan,* 2012). Orbital remote sensing across a wide wavelength scale (VNIR–TIR) indicates numerous occurrences of sedimentary minerals in ancient layered sequences including a variety of clays (e.g., nontronite, kaolinite) and chemically deposited constituents of likely sedimentary origin (Mg-, Ca-, Fe-sulfates, amorphous silica, iron oxides, chlorides, perchlorates) (*Bibring et al.,* 2006, 2007; *Murchie et al.,* 2009). The late Noachian–early Hesperian Burns formation at Meridiani Planum consists of Mg-Ca-Fe-sulfate cemented aeolian sandstones also containing amorphous silica and altered basalt (*Squyres et al.,* 2004; *Clark et al.,* 2005; *McLennan et al.,* 2005; *Glotch et al.,* 2006) and this secondary mineralogy is broadly consistent with that predicted from experimental and theoretical modeling studies of basalt alteration under low pH conditions (*Tosca et al.,* 2004, 2005; *Tosca and McLennan,* 2006).

Accordingly, two aspects of martian weathering appear to differ fundamentally from our terrestrial experience. As discussed above, the basaltic martian upper crust is profoundly different from the granodioritic terrestrial upper continental crust, both chemically and mineralogically, and this has direct implications for the composition of weathering profiles, clastic sediments, aqueous weathering fluids, and chemical sediments throughout the geological history of Mars. In post-Noachian terrains there is evidence that low-pH aqueous conditions typically were prevalent, resulting in a number of very distinct weathering reactions that typically are not observed during terrestrial weathering.

The presence of clay-bearing strata in Noachian terrains suggests that some form of weathering has proceeded throughout martian geological time. Noachian clays are dominated by Fe-Mg smectites (e.g., nontronite) with lesser more aluminous smectites and highly aluminous kaolinite. Their origin, and thus implications for understanding source-to-sink processes, is not well constrained and could be due to a variety of processes, including pedogenic weathering, *in situ* alteration (analogous to terrestrial bentonites), diagenesis, and/or hydrothermal alteration associated with volcanism and/or impacts. In addition, comparisons with terrestrial conditions are also complicated by a variety of other differences between the two planets that could influence aqueous alteration styles and rates, such as tectonics, vegetation, and atmospheric composition.

Assuming that at least some martian clays were derived from surficial weathering, the Fe-Mg smectites could be consistent with relatively low water/rock ratios (i.e., arid conditions) since in well-drained basaltic soils with high throughput of weathering fluids, more aluminous clays, notably kaolinite, would be expected (e.g., *White,* 1995; *van der Weijden and Pacheco,* 2003; *Milliken and Bish,* 2010; *Ehlmann et al.,* 2011). Another possibility is that clay minerals, formed in low water/rock ratio aqueous environments, could be then later transported and deposited in water-dominated fluvial and lacustrine environments (*Milliken and Bish,* 2010).

Toward the end of Noachian time the character of secondary mineralogy changed dramatically from being clay-dominated to being sulfate- and iron oxide-dominated (*Bibring et al.,* 2006) and this may have had an important effect on chemical weathering and other sedimentary processes. The change has been attributed to the acidification, oxidation, and desiccation of the martian surface and may be preserved in the stratigraphic record of Mars, e.g., at Gale Crater's Mount Sharp (*Milliken et al.,* 2010; *Grotzinger and Milliken,* 2012). One of the major objectives of the Mars Science Laboratory mission to Gale Crater is to investigate

this transition (*Grotzinger,* 2009; *Grotzinger et al.,* 2012). The nature of chemical weathering thought to dominate from the late Noachian is illustrated on A-CNK-FM ternary diagrams and compared to weathering of basalts under terrestrial conditions in Fig. 8. Under the circumneutral pH and oxidizing terrestrial conditions, weathering residues are concentrated in insoluble Al and Fe^{3+} and natural waters in turn are Al- and Fe-depleted (Figs. 8a,b). Accordingly, terrestrial weathering profiles and siliciclastic sediments derived from basaltic weathering regimes have compositions that scatter above the feldspar–(FeO_T + MgO) join on the A-CNK-FM diagram.

On the other hand, most altered rock and sediment analyzed on Mars (soils, altered rock surfaces, and sedimentary rocks) scatter parallel to and below the feldspar–(FeO_T + MgO) join (Fig. 8c). This trend is consistent with acidic alteration experiments (pH < 5) where mafic minerals (olivine, Fe-Ti oxides, pyroxene, glass) are more readily dissolved rather than altered to clays (Fig. 8d) (*Tosca et al.,* 2004; *Golden et al.,* 2005; *Hurowitz et al.,* 2005, 2006). Lack of evidence for Al-mobility, e.g., absence of Al-sulfates that might be expected in acidic environments that produced Fe^{3+}-sulfates (e.g., jarosite), led *Hurowitz and McLennan* (2007) to suggest that low water/rock ratios were involved so that only relatively soluble minerals (e.g, olivine but not plagioclase) were mainly affected.

3.3.2. Physical processes. Physical weathering on Mars differs as much in style as in degree compared to Earth. In addition to the increased role of impact processes in generating sedimentary particles, discussed above, the common occurrence of aeolian features and presence of polar ice caps also point to the importance of aeolian saltation abrasion and various glacial and permafrost processes. These were also likely important in the geological past as suggested, e.g., by the aeolian origin for the late Noachian–early Hesperian Burns formation (*Grotzinger et al.,* 2005). Widespread evidence for ancient channels on the martian surface also point to fluvial erosion of bedrock driven by saltation abrasion during aqueous transport. Section 4 will discuss these aspects in more detail.

It may be possible to provide some qualitative constraints on the relative roles of physical vs. chemical weathering on Mars if we assume that present-day soils reflect some time-integrated record of sedimentary processes. *McGlynn et al.* (2012) recently modeled the mineralogy of martian soils at Gusev Crater and Meridiani Planum and concluded that the chemical constituents (sulfates, chlorides, amorphous silica) represent ~15% of the soil. This is perhaps a surprising result since the terrestrial Phanerozoic sedimentary rock record (*Garrels and Mackenzie,* 1971) similarly contains ~18% chemical constituents (carbonate, evaporite, silica). As discussed above, impact processes were likely an efficient mechanism for producing sediment on Mars, suggesting that chemical weathering processes may be of less importance. However, balanced against that is the fact that basaltic minerals such as olivine, pyroxene, and Fe-Ti-oxides tend to dissolve more readily during chemical weathering (Table 2) and form a combination of dissolved constituents (Mg, Fe, Ca) and amorphous silica. In comparison, the bulk of the minerals in terrestrial continental crust (quartz, plagioclase, K-feldspar) are either resistant to chemical weathering (quartz) or form a lesser proportion of dissolved constituents and a larger proportion of resistant clays (plagioclase, K-feldspar) (*McLennan,* 2003).

3.4. Weathering on Venus

On Venus, where surface water is essentially absent, experiments indicate that the hot (~735 K), dense (72 kg/m^3), and dry (~30 ppm H_2O) CO_2-N_2-SO_2 atmosphere (Table 1) will interact directly with surface basalts to form a host of potential secondary minerals (e.g., anhydrite, pyrite, magnesite, magnetite), although details have yet to be confirmed by *in situ* measurements (*Johnson and Fegley,* 2002). The large ranges in surface temperature (627–753 K), pressure (4.5–11 MPa), and air density (36–74 kg/m^3) associated with different altitudes (–2 to +11 km) may allow for differences in the rates and types of chemical weathering across the venusian surface (*Basilevsky and Head,* 1993). Images from the Venera landers indicate substantial physical disruption of the basaltic surface (*Florensky et al.,* 1977; *Basilevsky et al.,* 1985), perhaps facilitated by chemical reactions, and formation of sedimentary particles that in turn may be involved in aeolian processes (*Craddock,* 2011), although yardangs and dune deposits appear uncommon (*Greeley et al.,* 1995) (see section 4. 2 below for further discussion).

It is likely that the role of impacts in facilitating physical weathering on Venus is limited, although the two dune fields identified on the surface are found in close association with large impacts, suggesting their ejecta supplied the dune-forming sediment (*Greeley et al.,* 1995). Regardless, Venus was entirely resurfaced by basaltic volcanism at about 1.0–0.85 Ga and there are only about 940 craters on the surface, approximately equal to the terrestrial record over the same period of time (*Taylor and McLennan,* 2009). In addition, the filtering effects of the very thick atmosphere results in no basins <5 km in diameter and few <30 km being formed. The thick atmosphere also limits the transport of ejecta blankets and for many of the craters that are present, parts of the ejecta blankets are entirely missing due to complex atmospheric interactions. Venusian craters are mostly highly pristine with little evidence for significant erosion and degradation.

3.5. Weathering on Titan

Titan's cold (~95 K) surface (Table 1) is composed of an unknown mixture of crystalline water ice, clathrate hydrate, and solid organics, with perhaps a minor component of ammonia-rich ices (*Lorenz and Lunine,* 2005). There are few impact craters on the surface, indicating that it is relatively young (*Wood et al.,* 2010; *Neish et al.,* 2013). The atmosphere is dense (0.15 MPa, 5 kg/m^3) and nitrogen-based, with a volumetric concentration of ~5% methane at the surface (*Lunine and Atreya,* 2008) (Table 1). A low

adiabatic lapse rate (~1 K/km) and 2–3 K diurnal and seasonal temperature variations (*Jennings et al.,* 2009, 2011) suggest that physical weathering mechanisms involving freeze/thaw cycles and/or variations in thermal stress are thermodynamically improbable. The insolubility of water ice in liquid methane and ethane ($<10^{-11}$ mole fraction) argues against dissolution-based chemical weathering of water-ice bedrock (*Lorenz and Lunine,* 1996; *Perron et al.,* 2006), despite the observation of karst-like morphologies (e.g., *Hayes et al.,* 2008; *Mitchell et al.,* 2007) and an abundance of topographically closed depressions in the polar regions (*Hayes et al.,* 2013). Regardless, the abundance of aeolian dunes in Titan's equatorial regions indicates that sedimentary particles are being produced (see section 5.2.3 and Fig. 14d below).

A unique sediment production mechanism on Titan

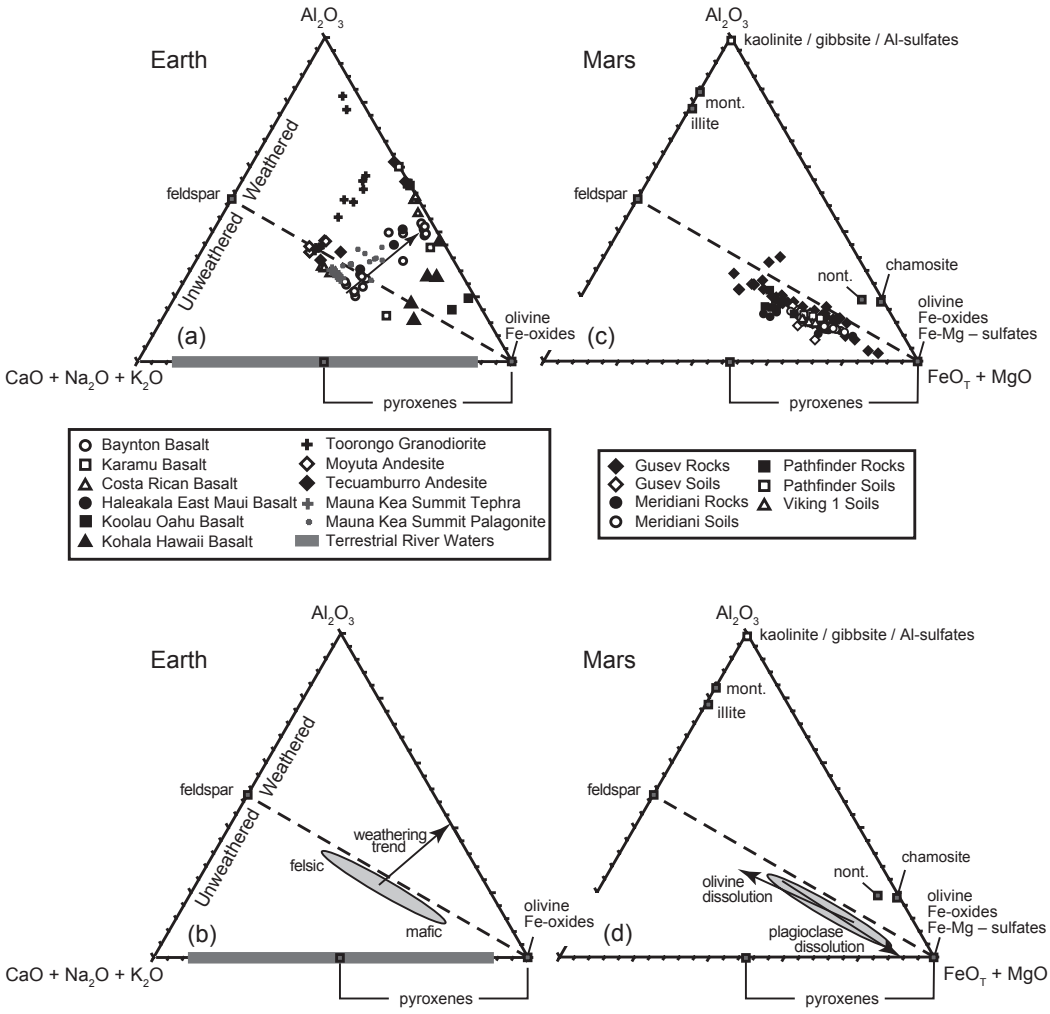

Fig. 8. Ternary diagrams plotting molar proportions Al_2O_3–($CaO + Na_2O + K_2O$)–($FeO_T + MgO$), or A-CNK-FM, comparing basaltic weathering trends on Earth and Mars. In this case, no corrections are made for nonsilicate components. Selected igneous and sedimentary minerals are plotted and the dashed diagonal lines connect feldspars to the FM apex, effectively separating the lower part of the diagrams dominated by primary igneous minerals (unweathered) from the upper parts dominated by clays (weathered). **(a)** Weathering and alteration profiles in terrestrial basaltic-andesitic settings illustrating that increased alteration results in enrichment insoluble Al and Fe and concentration in residual clays and oxides. **(b)** Schematic diagram showing compositional variation in primary terrestrial igneous rocks with an arrow indicating a typical terrestrial weathering trend. **(c)** Martian soils, igneous rocks, altered rock surfaces, and sedimentary rocks. Almost all data fall below and parallel to the diagonal line in spite of widespread evidence for alteration. **(d)** Schematic diagram showing compositional variation in martian mafic to ultramafic igneous rocks with arrows showing trends for olivine and plagioclase dissolution from typical basalt. Differing trends for terrestrial and martian alteration patterns can be explained by low-pH, low-water/rock ratio conditions on Mars whereby mineral dissolution dominates over alteration to clays. Adapted from *Hurowitz and McLennan* (2007) and *McLennan* (2012).

involves organic particulates that are generated through methane photolysis in the upper atmosphere (*Yung et al.,* 1984). While the particles settling out from the atmosphere are likely too small to saltate, they may form aggregates or crusts that can be eroded into saltatable-sized particles of ~200 μm (*Lorenz et al.,* 2006). Another Titan-specific process involves the interaction between ice and liquid alkane. Recent experiments have shown water-ice is wettable (lyophilic) to methane and ethane under Titan-relevant conditions, allowing liquid alkanes to be absorbed into the ice and potentially cause changes to both its optical and physical properties (*Sotin et al.,* 2009). If there is an associated volume change, repeated wetting and drying events may weaken water ice in a physical weathering mechanism analogous to terrestrial rock disintegration. While water ice is insoluble in liquid methane and ethane, constituents of the complex organic sediments generated through photolysis (e.g., acetylene) may have sufficient solubility to generate dissolution features given sufficient abundance and time (*Mitchell and Malaska,* 2011). The recent observation of potential evaporite deposits found in the floors of empty lake basins (*Barnes et al.,* 2011) further support the plausibility of dissolution chemistry on Titan.

In addition to the soluble components of the complex hydrocarbons and nitriles generated in the upper atmosphere, the solubility of pure ammonia ice may approach that of calcium carbonate on Earth (10^{-5}–10^{-6} mole fraction), although measurement uncertainties of ammonia ice solubility at 94 K cover three orders of magnitude (*Perron et al.,* 2006). While thermodynamic equilibrium would require ammonia ice to be in the form of ammonia-water hydrates on Titan (*Perron et al.,* 2006), disequilibrium mixtures containing pure ammonia ice can be formed by flash freezing, as might be expected during an ammonia-water cryovolcanic event (*Yarger et al.,* 1993). Finally, methanol has been suggested as a minor component of Titan's primordial ocean (*Deschamps et al.,* 2010). If methanol can be brought to the surface, it would also be soluble in liquid alkane. If Titan's surface contains a significant contribution of any of these soluble materials, chemical weathering may be important.

4. SEDIMENT PRODUCTION

Sediment production is the process of breakdown of rock or immobile regolith into mobile particles. There are a host of potential processes involved in sediment production. In addition to chemical and physical weathering (see above), scour by flowing fluids (e.g., wind, rivers, or glaciers) and the sediment they transport, hillslope processes (e.g., landslides, debris flows, and soil creep), and impact cratering can be important for producing sediment. Although many processes may be important, Earth, Mars, and Titan all show convincing evidence for sediment production and large-scale transport by rivers, and including Venus, all four bodies show evidence for wind erosion and transport. Here we focus on sediment production and erosion by rivers and wind.

4.1. Fluvial Bedrock Erosion

Fluvial bedrock erosion is one of the main drivers of landscape evolution on Earth; in addition, similar processes appear active on Titan, and were likely important in the martian past. For example, patterns of ancient river networks on Mars have been used to infer volatile sources and as evidence for precipitation. Dendritic drainage patterns suggest distributed fluid source areas such as rainfall or snowmelt in some places (e.g., *Mangold et al.,* 2004), whereas in other places large anabranching bedrock valleys with inner gorges, cataracts, and streamlined islands suggest catastrophic outburst flooding (*Baker,* 1982). Longitudinal valley networks with stubby amphitheater-headed tributary channels often are inferred to represent erosion from groundwater seepage (*Sharp and Malin,* 1975; *Carr and Clow,* 1981). However, similar valley shapes more often occur on Earth due to headwall undermining or collapse from waterfall processes (*Lamb et al.,* 2006, 2008a). Like Mars and Earth, the surface of Titan shows evidence for dendritic drainage networks and valley networks with stubby tributary heads (e.g., *Burr et al.,* 2013), but it lacks apparent outburst-flooding features (*Burr,* 2010).

Fluvial processes have been considered a possibility on the surface of Venus. Although there are more than 200 channels preserved on the plains of Venus, many >500 km in length and a few with deltas, they typically are smooth at a centimeter scale with no boulders, as characterized by radar. These channels are best interpreted to represent erosion by low-viscosity lava flows (*Baker et al.,* 1992).

Rivers can be divided into those that are supply-limited or transport-limited with respect to sediment supply (section 2.1). Supply-limited rivers typically have a flux of sediment q_s (per unit channel width) that is less than the transport capacity (i.e., $q_s < q_{sc}$), and partial exposure of bedrock on their beds. These rivers tend to be net erosional and this is where sediment is produced. River erosion into bedrock typically occurs by plucking of jointed fragments of rock and abrasion from impacting sediment (*Whipple et al.,* 2000). Although dissolution may play a role in some cases (e.g., carbonates on Earth, sulfates on Mars, and ice bedrock on Titan may dissolve in certain hydrocarbon mixtures), it is generally thought to be a minor component of fluvial bedrock erosion on all three bodies (e.g., *Whipple,* 2004; *Perron et al.,* 2006). A host of incision mechanisms can occur at migrating knickpoints and waterfalls, including plunge-pool scour, undercutting, seepage, and block toppling (e.g., *Whipple,* 2004; *Williams and Malin,* 2004; *Lamb et al.,* 2006; *Lamb and Dietrich,* 2009; *Warner et al.,* 2010).

The mechanics of river bed incision by plucking and abrasion were recently reviewed by *Burr et al.* (2013) for Earth and Titan, and are summarized here. Plucking is a process of removal of blocks of rock from a river bed and is typically modeled as a function of bed shear stress (τ_b) in excess of the threshold stress (τ_c) required for motion (*Hancock,* 1998; *Whipple et al.,* 2000). This makes erosion by plucking extremely sensitive to joint patterns in rock at

meter or submeter scale (e.g., *Whipple et al.,* 2000; *Lamb and Fonstad,* 2010), and therefore predictions are difficult on Titan and Mars where fine-scale joint patterns cannot readily be measured. Models for river-bed abrasion are based on particle impacts of the bed by saltating and suspended sediment (*Sklar and Dietrich,* 2004; *Lamb et al.,* 2008b). Abrasion ceases when the sediment supply exceeds the transport capacity (i.e., $q_s > q_{sc}$) because deposition protects the underlying bedrock from erosion. In abrasion models, the erosion rate is a function of rock strength, bed shear stress, sediment supply, and the capacity of the river to transport sediment (*Sklar and Dietrich,* 2001). Abrasion models can be scaled for Mars and Titan (*Collins,* 2005; *Burr et al.,* 2013), and estimates for Titan, for example, show that incision rates predicted by a saltation-abrasion model, for fixed channel geometry and sediment conditions at Titan temperatures, are about 40 times less than on Earth for terrestrial rock of similar strength (*Sklar,* 2012). The strength of ice, and thus its resistance to erosion, also depends on crystal grain size and the concentration of solid impurities, both of which are poorly constrained on Titan (*Litwin et al.,* 2012).

4.2. Wind Erosion

Aeolian erosion occurs primarily through deflation, the removal and transport of loosened material, and abrasion, the mechanical wear of coherent material (*Anderson,* 1986). Morphologies that result from aeolian erosion include wind streaks, ventifacts, yardangs, deflation basins and pans, and inverted relief *(Laity,* 2011). Ventifacts, or wind-abraded rocks, have been observed on Earth and Mars (*Laity and Bridges,* 2009), while wind streaks, yardangs, and deflation basins have been reported on Venus, Earth, Mars, and Titan (*Greeley and Iversen,* 1987; *Greeley et al.,* 1995; *Bourke et al.,* 2010). Sediment piles that collected on the Venera 13 spacecraft during landing on Venus were observed to deflate due to near-surface winds during the hour following touchdown (*Selivanov et al.,* 1982), also suggesting active aeolian processes. Inverted relief resulting from differential erosion between fluvial and/or volcanic channel deposits and their surrounding terrain are observed on Earth and Mars (*Pain et al.,* 2007). Aeolian erosion is also one of the primary mechanisms of dust formation. Dust concentrations have far-reaching importance on a planetary surface, influencing geomorphologic processes, atmosphere conditions, and the planetary stratigraphic record (*Grotzinger and Milliken,* 2012; *Farmer,* 1993).

Physical weathering rates on Mars are difficult to determine with any precision and likely changed dramatically over geological time with an episodic reduction in rates at about the end of Noachian time. Similarly, relatively little work has been done to evaluate the full range of processes that may have been responsible for erosion and denudation of the planet (*Malin,* 1974; *Chan et al.,* 2008; *Viles et al.,* 2010). Diurnal thermal cycling, involving low temperatures and temperature differences of >75°C or more, undoubtedly plays a significant role (*Leask and Wilson,* 2003; *Viles et al.,* 2010), comparable to the most extreme deserts on Earth.

The rate of aeolian abrasion can be estimated by the multiplication of materials susceptibility to erosion (S_a), the particle flux of entrained aeolian material (q), and the wind frequency above the saltation threshold (f). *Greeley et al.* (1982) predicted the abrasion rate at the Viking 1 landing site on Mars to be up to ~210 μm per year using measured meteorological data, significantly greater than expected considering the age of the surface determined by crater counting and interpreted as evidence for a lack of sand-sized material. *In situ* estimates of current erosion rates in Gusev Crater and on Meridiani Planum, using a variety of approaches (e.g., lags of resistant hematitic concretions, deflation under rocks), indicate <10 nm/yr and mostly <1 nm/yr or $>10^2$ times (and up to 10^5 times) slower than any denudation rate measured on Earth (*Golombek et al.,* 2006). *Carr and Head* (2010) reviewed the literature on martian denudation rates over geological time and concluded that the highest average rates in the Noachian (which includes both fluvial and aeolian erosion), at ~5 m/10^6yr (~5000 nm/yr), were comparable to or less than denudation rates on highly stabilized terrestrial cratons. The end of Noachian time marked a fundamental shift in physical weathering processes with a drop of some 4–5 orders of magnitude, leading to average Hesperian/Amazonian rates of ~2–3 × 10^{-5} m/10^6yr (~0.02–0.03 nm/yr). Most recently, *Bridges et al.* (2012) used measurements of dune migration in the Nili Patera dune field, Mars, to model abrasion and derived modest rates of 1–10 μm/yr for flat ground and of 10–50 μm/yr for vertical rock faces, similar to basalt abrasion rates in Antarctica's Victoria Valley on Earth of 30–50 μm/yr (*Malin,* 1986).

5. SEDIMENT TRANSPORT

Earth, Mars, Titan, and Venus show evidence for large-scale transport of sediment from source areas to depositional sinks. Fluvial and aeolian processes are likely the most significant mechanisms for large-scale sediment transport and also represent important components of planetary climate. Detailed study of both modern and ancient fluvial and aeolian deposits can reveal information regarding both past and present atmospheric conditions.

5.1. Fluvial Sediment Transport

River valleys on Titan and Mars, and observations of rounded grains in a putative river plain at the Huygens landing site on Titan (*Tomasko et al.,* 2005), suggest that sediment has moved within rivers on both planetary bodies. The best-developed quantitative theories for sediment transport are for rivers with their bed and banks composed of unconsolidated sediment (i.e., alluvial rivers), rather than bedrock. Unlike net-erosional, supply-limited rivers discussed in section 4.1, alluvial rivers tend to be net depositional or bypass sediment over geologic timescales. In this case, the sediment flux is determined by the capac-

ity of the flow to transport the material (i.e., $q_s = q_{sc}$), rather than erosion from bedrock, and sediment flux can be predicted relatively accurately from flow hydraulics and sediment size. It is instructive to consider the dynamics of channelized fluid flow before discussing sediment transport.

5.1.1. Flow dynamics. Flow of a Newtonian fluid in a channel can be modeled through conservation equations for fluid mass and momentum and a parameterization for bed friction (e.g., a turbulence drag law) (e.g., see *Burr et al.,* 2013, for a recent review). For depth-averaged, Reynolds-averaged conditions in a wide channel, these equations are $Q = Uhw$, $\tau_{bd} = \rho ghS$, and $\tau_b = \rho C_f U^2$, where Q is the volumetric fluid flux, U is the depth-averaged flow velocity, h is the flow depth, w is the channel width, τ_{bd} is the driving stress acting on the river bed due to gravitational acceleration of the fluid, τ_b is the shear stress acting on the bed due to friction, ρ is the fluid density, g is gravitational acceleration, S is the dimensionless bed slope gradient, and C_f is a dimensionless friction coefficient (e.g., *Chow,* 1959). For many river systems, the flow is approximately steady and uniform flow, i.e., $\tau_b = \tau_{bd}$ (e.g., *Parker et al.*, 2007), and therefore the conservation equations can be combined as $Q = wh(ghS/C_f)^{1/2}$. This analysis shows that, at bankfull conditions, the fluid discharge can be calculated from measurements of channel depth, width and slope, and the bed friction coefficient. The bed friction coefficient is a function of the fluid viscosity only for laminar or hydraulically smooth flows (*Nikuradse,* 1933; *Schlichting,* 1979; *Garcia,* 2007), conditions that are unlikely for most rivers on Earth, Mars, and Titan where w > 1 m and D > 1 mm (or the bed contains bedforms; section 5.1.2) (e.g., *Perron et al.,* 2006; *Burr et al.,* 2013). For turbulent, hydraulically rough flow, C_f depends on the ratio of the flow depth to the bed-roughness length scale (e.g., *Parker,* 1991). Together, these equations can be used to calculate possible river discharges on Earth, Mars, and Titan (*Burr et al.,* 2002; *Irwin et al.,* 2004; *Perron et al.,* 2006; *Lorenz et al.,* 2008). Hydraulic equations developed for water on Earth should be directly applicable to Mars and Titan when differences in gravity and fluid density are taken into account. One of the biggest limitations in applying these hydraulic equations is identification of river channel width (w) rather than valley width, the latter of which can be orders of magnitude larger than the former.

5.1.2. Sediment transport. The motion of fluid in a river imparts a shear stress on the river bed. Once a critical shear stress is surpassed, sediment begins to move as bed load by rolling and bouncing along the riverbed. For noncohesive sediment, the criterion for sediment motion can be calculated from the nondimensional bed-shear stress, or Shields stress, $\tau_* = \tau_b/[(\rho_s - \rho)gD]$. For small particle Reynolds numbers [$Re_p = [(rgD)^{1/2}D/\nu]$, where $r = (\rho_s - \rho)/\rho$ is the submerged specific density of the sediment, and ρ_s and ρ are the densities of sediment and fluid, respectively], the critical value of the Shields stress, τ_{*c}, for incipient motion, varies with the particle Reynolds number, and therefore fluid viscosity (*Shields,* 1936). For large particle Reynolds numbers ($Re_p > 10^2$) and for shallow channel slopes (S < 0.05), $\tau_{*c} \approx 0.045$ (*Miller et al.,* 1977; *Wilcock,* 1993), and sediment motion is independent of fluid viscosity. This corresponds to sediment motion for D > ~1 mm (i.e., $Re_p > 10^2$) for conditions on Earth, Mars, and Titan, assuming values for siliceous grains in water on Earth and Mars [r = 1.65 (e.g., quartz on Earth; plagioclase on Mars), $\nu = 10^{-6}$ m^2/s, and g = 9.81 m/s^2 and g = 3.73 m/s^2 for Earth and Mars, respectively], and r = 1.18, g = 1.35 m/s^2, and $\nu = 4 \times 10^{-7}$ m^2/s for transport of water-ice sediment by flowing methane on Titan (e.g., *Burr et al.,* 2006, 2013; *Perron et al.,* 2006) (see also Table 1). On steep slopes (S > 5%), τ_{*c} can increase by as much as an order of magnitude due to particle emergence and changes to the structure of the flow (e.g., *Lamb et al.,* 2008c). In river beds with mixtures of sediment sizes, which may exist on Titan (*Tomasko et al.,* 2005), the statistics of the mixture (e.g., median particle size) and particle-size bimodality can influence incipient motion conditions (e.g., *Parker,* 1990; *Wilcock and Crowe,* 2003). In addition, cohesion may influence incipient sediment motion for very fine particles (e.g., D > 0.05 mm), and for organic sediment particles on Titan (*Rubin and Hesp,* 2009).

Sediment is suspended within the flow at large flow velocities and for small particles, when the settling velocity of a particles is less than the magnitude of turbulent velocity fluctuations within the fluid, or $u_* \equiv \sqrt{\tau_b/\rho} > 0.8w_s$, where u_* is the bed-shear velocity and w_s is the particle-settling velocity (*Bagnold,* 1966). Empirical settling-velocity equations (e.g., *Dietrich,* 1982) explicitly account for particle and fluid densities, fluid viscosity, and gravity, making them straightforward to apply to different fluids and planetary bodies.

Stability fields for each of the three sediment transport conditions (no motion, bed load, and suspended load) are functions of the particle diameter and bed shear stress for a given transport system (Fig. 9). Stability fields are shifted in different systems as a function of gravity, particle density, fluid density, and viscosity (e.g., *Komar,* 1980; *Burr et al.,* 2006). For Earth and Mars, we make the calculation for silicious grains in water (r = 1.65, $\nu = 10^{-6}$ m^2/s), where the shift in transport conditions is due only to differences in gravity (g = 9.81 m/s^2 and g = 3.73 m/s^2 for Earth and Mars, respectively) (Table 1). This results in a reduction of the necessary bed shear stress to transport particles and initiate suspension on Mars relative to Earth. Following *Lamb et al.* (2012), a second case is shown for Mars for the case of viscous brines, which have been inferred to be important in transporting sediment in some environments on Mars due to the observation of sediment mineral phases that are highly soluble in fresh water (*McLennan et al.,* 2005; *Tosca et al.,* 2011). Given one of the most viscous brines considered by *Tosca et al.* (2011) (r = 1.04 and $\nu = 4 \times 10^{-5}$ m^2/s; Table 1), this shifts the transport thresholds to substantially coarser particle sizes. Thus, grains as large as a few millimeters transported in turbulent brines may be suspended once moved, owing to the reduced settling veloc-

ity in the high-viscosity fluid. Finally, following *Burr et al.* (2006), we show a case for water-ice particles transported by liquid methane on Titan (r = 1.18, g = 1.35 m/s^2, and $\nu = 4 \times 10^{-7}$ m^2/s; Table 1). Here the transport boundaries are shifted to much lower bed shear stresses primarily due to lower gravity on Titan as compared to Earth and Mars. The density of particles is uncertain on Titan, however, as Titan's river networks may contain organic tholin compounds (*Schröder and Keller,* 2008; *Janssen et al.,* 2009) with different transport properties depending on their porosity (e.g., *Burr et al.,* 2013).

5.1.3. Fluvial bedforms. In low-gradient (S < 1%), sand-bedded channels on Earth, river beds are not often flat, but instead contain bedforms such as ripples and dunes (e.g., *Southard,* 1991). These bedforms are important to consider for fluvial processes on Mars and Titan because they influence fluid-flow and sediment transport rates, and they leave distinct signatures in the sedimentary record (see section 6). Note that only conceptual models and empirical correlations are available for bedforms in steep (S > 1%) channels with coarse beds (e.g., *Montgomery and Buffington,* 1997), and their application to other planetary bodies is uncertain.

Lamb et al. (2012) compiled results from five sediment transport and bedform studies (*Chabert and Chauvin,* 1963; *White,* 1970; *Brownlie,* 1983; *Southard and Boguchwal,* 1990a; *van den Berg and van Gelder,* 1993) to build a comprehensive bedform stability diagram for subcritical flows (Fr < 1, where $Fr = U/\sqrt{gh}$ is the Froude number) that spans a large range in particle Reynolds number, Re_p (Fig. 10a). The compilation shows that bedform phase space, like incipient sediment motion, can be cast as a function of the Shields stress, τ_*, and Re_p. At low Shields stresses, sediment is immobile (Figs. 9, 10a). At higher Shields stresses sediment is mobile and the bed may take on a number of states: Ripples form at low Re_p and moderate values of τ_*, whereas at higher Re_p lower plane bed and dunes are stable (Fig. 10a). For all Re_p, the bed is planar (upper plane bed) for large values of the Shields stress.

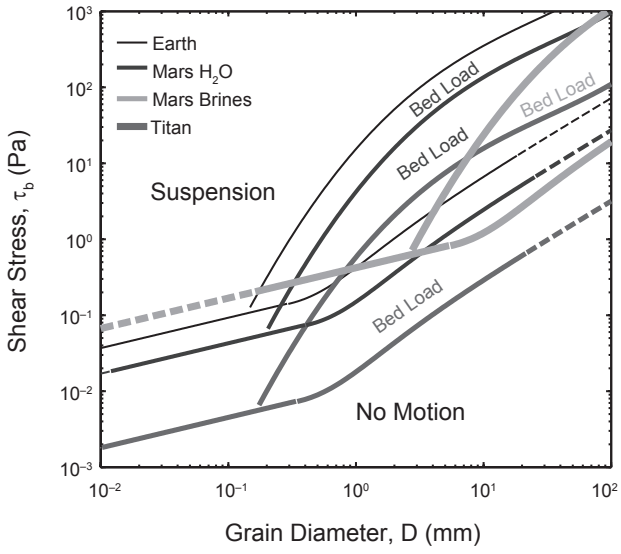

Fig. 9. Sediment transport diagram showing the bed shear stress required for initial motion and suspension for siliceous grains (e.g., quartz, feldspar) transported by water on Earth, siliceous grains (e.g., plagioclase) transported by water and viscous brines on Mars, and water-ice grains transported in methane on Titan. Labels "No Motion" and "Suspension" apply to all four cases. Following *Komar* (1980) and *Burr et al.* (2006).

Like the modes of sediment transport (Fig. 9), bedform state depends on fluid and particle densities, fluid viscosity, and gravity, which are different for fluvial processes on Mars, Titan, and Earth (e.g., *Southard and Bogouchwal,* 1990b). Following application of the bedform state diagram (Fig. 10a) to Mars by *Lamb et al.* (2012) and Titan by *Burr et al.* (2013), we illustrate these differences for the cases of silicious grains in water on Earth (r = 1.65, $\nu = 10^{-6}$ m^2/s, and g = 9.81 m/s^2), silicious grains in viscous brines on Mars (r = 1.04, $\nu = 4 \times 10^{-5}$ m^2/s, and g = 3.73 m/s^2), and water-ice grains in liquid methane on Titan (r = 1.18, g = 1.35 m/s^2, and $\nu = 4 \times 10^{-7}$ m^2/s) (Table 1) (Figs. 10b,c). Bedform stability under flowing martian brines is shifted to coarser sediment sizes as compared to freshwater flows on Earth (Fig. 10b). This is primarily due to the 40-fold increase in fluid viscosity, which affects the particle Reynolds number. For example, ripples on Earth only occur for relatively fine particles (D < 1 mm), whereas martian brines may produce ripples in sediment sizes up to 20 mm (Fig. 10b) (*Lamb et al.,* 2012). The bedform stability is shifted to much lower bed stresses on Titan as compared to Earth (Fig. 10c). This results from the 10-fold reduction in the submerged specific weight of sediment (i.e., rg) that affects the Shields stress. For example, at the bed stresses necessary for initial motion of 0.1-mm diameter sediment on Earth, the bed state on Titan is predicted to be upper-plane bed (Fig. 10c) (*Burr et al.,* 2013).

5.2. Aeolian Sediment Transport

Aeolian landforms, such as dunes, wind streaks, and yardangs, have been observed on the surfaces of Earth, Mars, Titan, and Venus (e.g., *Bourke et al.,* 2010). The ubiquitous presence of these features suggests that the entrainment, transport, and deposition of sediment by wind are important geomorphic processes that operate in arid regions across the solar system. Unlike the fluvial processes described above, which are currently active on Earth and Titan, it is likely that aeolian processes are active on all four bodies. Aeolian transport involves interactions between the wind and ground surface, resulting in a strong dependence on textural and surficial conditions (e.g., surface crusts, surface moisture, and vegetation cover). Grain size is also important, leading to fundamental differences in the processes responsible for the entrainment, transport, and deposition of large (sand-sized or greater) vs. small (silt, clay, and dust) particles. Similar to flow in rivers, aeolian systems operate in both

transport and supply limited regimes; however, most aeolian environments on Earth tend to be supply limited (*Nickling and Neuman,* 2009). In supply-limited systems flux is determined by sediment availability, or the rate at which the surface can supply grains to the air stream. Many natural surfaces exhibit spatial and/or temporal variations in surface and/or atmospheric conditions that can limit sediment availability (*Kocurek and Lancaster,* 1999).

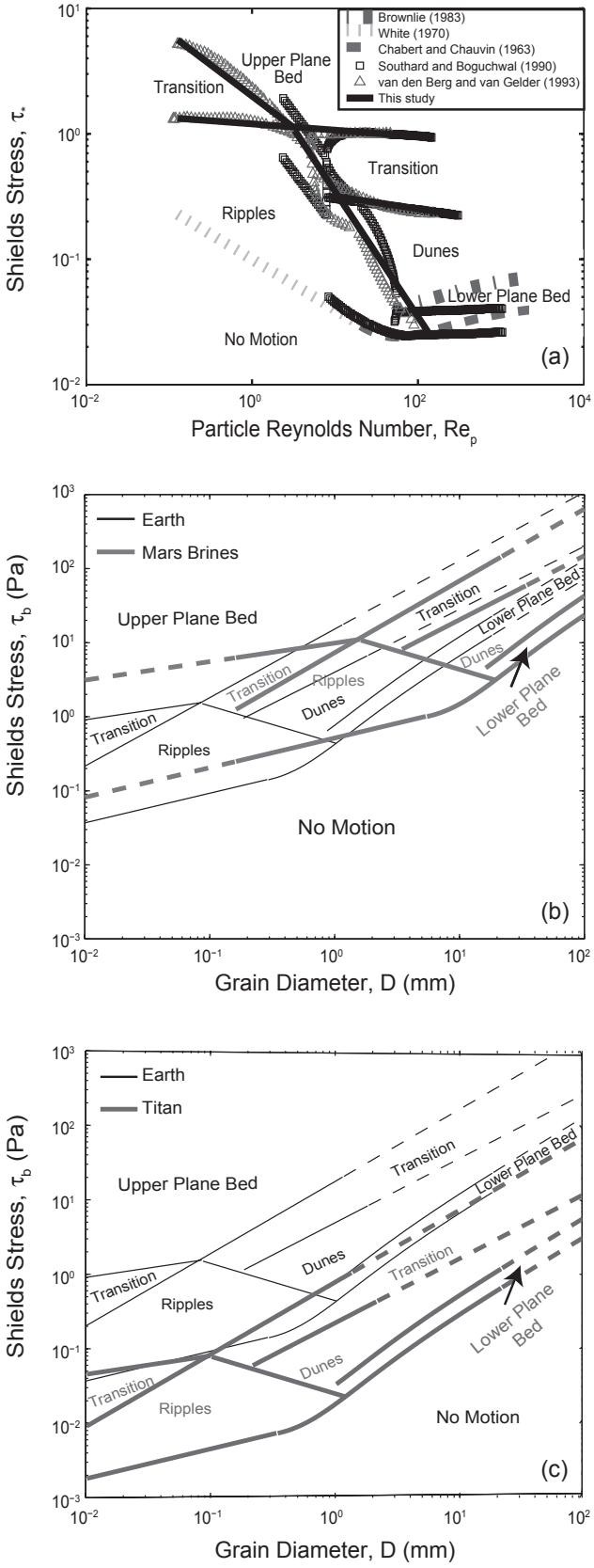

Fig. 10. Stable bedform states. **(a)** Bed states as a function of the Shields stress and particle Reynolds number (modified after *Lamb et al.,* 2012; *Burr et al.,* 2013). Solid lines are best-fit boundaries between bed states that summarize findings from five previous studies (*Chabert and Chauvin,* 1963; *White,* 1970; *Brownlie,* 1983; *Southard and Boguchwal,* 1990a; *van den Berg and van Gelder,* 1993). Stable bed states as a function of bed-shear stress and particle diameter for the cases of **(b)** viscous brines transporting siliceous grains on Mars and freshwater flows transporting siliceous grains on Earth (modified after *Lamb et al.,* 2012), and **(c)** water-ice particles on Titan and freshwater flows transporting siliceous grains on Earth (modified after *Burr et al.,* 2013). Dashed lines are power-law extrapolations of stability boundaries from **(a)**. Labels "Upper Plane Bed" and "No Motion" apply to all three cases.

5.2.1. Flow dynamics. Like the river processes described in section 5.1, the wind also exerts a bed shear stress on a planet's surface. The bed shear stress, τ_b, or bed shear velocity $\left(u_* \equiv \sqrt{\tau_b/\rho}\right)$, can be related to the wind velocity, U, at a given height above the bed, z, using a drag law, e.g., the commonly used log law $(U/u_*) = [(1/\kappa)\ln(z/z_0)]$, where z_0 is a function of the bed roughness for hydraulically rough flow (see section 5.1.2). Once the threshold for grain entrainment is surpassed, sediment moves in both bed load (saltation and creep) and suspended load, although saltation accounts for ~95% of the total mass transport in a typical aeolian system (*Nickling and Neuman,* 2009). This sediment is ultimately deposited to form bedforms such as loess, sand sheets, ripples, and dunes. During transport, momentum exchange between a developing saltation cloud and the wind results in a reduction of wind speed as the transport rate approaches a dynamic equilibrium known as steady-state saltation (*Anderson and Haff,* 1988). This equilibrium is typically reached within a few seconds of initial grain movement (*Nickling and Neuman,* 2009).

5.2.2. Sediment entrainment. Bagnold (1941) classified wind-driven particle motion into three modes with increasing wind speed: creep, saltation, and suspension (Fig. 11). There are no sharp distinctions between these transport modes; rather, they represent end members of a continuum. In aeolian systems, the specific mode of transport is often determined by the particle setting velocity (w_s) relative to the bed shear velocity (u_*). For low-particle Reynolds numbers ($Re_p < \sim 10$), the settling velocity is given by $w_s = \{[(\rho_p/\rho)-1]gd^2/(18\nu)\}$ (i.e., Stoke's Law). For high Reynolds numbers ($Re_p > \sim 100$), u_*/w_s can be recast in terms of $\tau_* = u_*^2/[(\rho_s-\rho)/\rho]gD$, which is typical in river sediment transport theories, since for this regime the particle settling velocity is proportional to $[(\rho_s-\rho)/\rho]gD$ and independent of viscosity (e.g., *Dietrich,* 1982).

Initial particle motion by saltation occurs when aerodynamic drag, lift, and moment surpass the restoring forces of gravity and interparticle forces (e.g., Van der Waals forces, soil moisture, surface crusts, etc.). For example, *Iversen and White* (1982) and *Iversen et al.* (1987) used wind tunnel experiments to empirically derive the critical Shields stress for grain entrainment, τ_{*c}, over a range of environments and found that it was primarily a function of the particle-friction Reynolds number, particle-to-fluid density ratio, and interparticle forces. *Shao and Lu* (2000) use the data from *Iversen and White* (1982) to derive an expression for τ_{*c} that is relevant for grain sizes that include sand: $\tau_{*c} \approx 0.012\,[1 + 3 \times 10^{-4}\,(\mathrm{kg/s^2})/(D^2\rho_s g)]$. Figure 12 shows this expression for a range of silicate grain sizes on Venus, Earth, and Mars, and for hydrocarbon grains for Titan. In all cases interparticle forces were assumed to be proportional to particle diameter following *Jordan* (1954), which was calibrated using silicate grains as described in *Iversen et al.* (1987). It should be noted that there is little known in regard to the cohesive behavior of water ice and/or hydrocarbon grains under Titan conditions and that *in situ* observation suggests that additional electrostatic forces may be important on Mars (*Sullivan et al.,* 2008). For large particles (D > ~200 μm), interparticle forces are negligible compared to gravity, whereas for small particles (D < ~70 μm), interparticle forces dominate (*Iversen et al.,* 1987). Venus and Titan have significantly lower thresholds for grain entrainment than Earth and Mars (Fig. 12). This difference results mainly from the high atmospheric density and viscosity on Venus and the high atmospheric density and low gravity on Titan, both of which reduce the effective settling velocity of particles. Titan's low atmospheric viscosity actually increases the settling velocity for small particles, although its effects are marginalized by the high density and low gravity.

Large particles ($w_s/u_* > 10$) (*Nino et al.,* 2003) are too big to be lifted by the wind. These particles are moved short distances by pushing and/or rolling in response to the impact of smaller grains in a process known as surface creep. At greater wind speeds (or smaller particle sizes) ($2.5 < w_s/u_* < 10$) (*Nishimura and Hunt,* 2000), grains are lifted into the wind and bounce across the surface following parabolic trajectories characteristic of aeolian saltation. Assuming the initial take off speed is on the order of the critical shear velocity (u_{*c}), *Almeida et al.* (2008) found that the characteristic saltation height, H_s, and length, L_s, are approximately $[H_s,L_s] \approx [81,1092](v^2/g)^{1/3}(u_*-u_{*c})/\sqrt{gD}$. On Earth and Titan, saltation heights are up to ~15 cm and lengths are ~2 m, while on Mars particles can follow trajectories with heights of up to ~5 m and lengths of ~120 m (*Almedia et al.,* 2008). Venus, as expected from its extremely low atmospheric viscosity (Table 1), has predicted saltation heights of ~1 cm and lengths of ~30 cm. Saltation often accounts for greater than 95% of the total mass transport in an aeolian system (*Nickling and Neuman,* 2009).

Initial saltating and creeping grains generate impact forces that set off a cascade effect that exponentially increases the number of grains entrained in the flow (*Nickling and Neuman,* 2009). Particle motion initiated by impact from saltating particles is known as splash, and the distribution of ejected particles is known as the splash function (*Ungar and Haff,* 1987). Saltating particles can also instigate suspension by ejecting finer-grained particles, which may be too cohesive to saltate on their own, into the atmosphere upon impact (*Chepil and Woodruff,* 1963).

Like particles in water, significant sediment suspension can occur when $w_s/u_* < \sim 1$ (*Nino et al.,* 2003). In wind, particles can be kept aloft for several days to weeks and

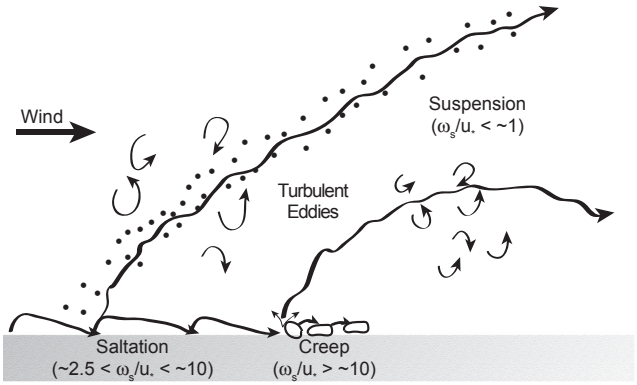

Fig. 11. Eolian sediment transport modes by wind (modified after *Pye,* 1987).

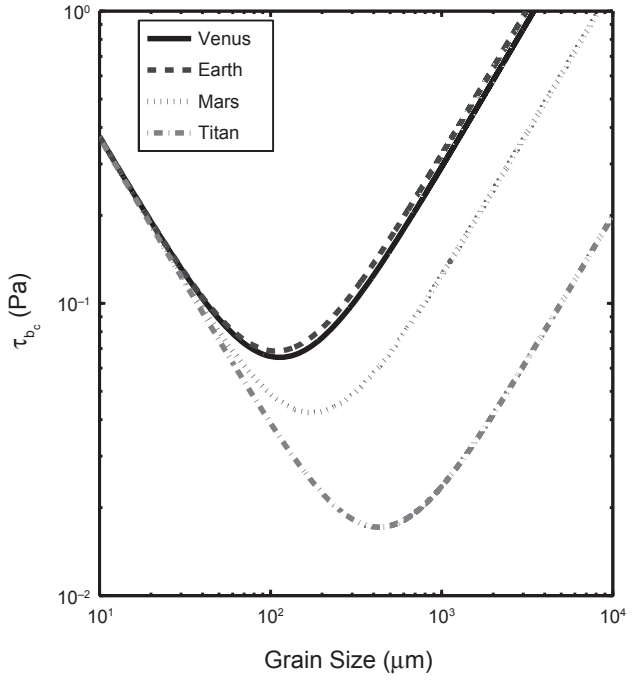

Fig. 12. Critical shear stress for eolian grain entrainment by saltation using the data from *Iversen and White* (1982) and equations presented in *Shao and Lu* (2000).

travel thousands of kilometers in a process called long-term suspension (*Tsoar and Pye,* 1987). On Mars, suspended particles of this type generate local, regional, and global dust storms that drape the surface in fine-grained material (e.g., *Greeley and Iversen,* 1987). Dust storms have significant environmental impacts on Earth, which include contaminating air quality, modifying soil composition, and contributing to the desertification of arid and semi-arid landscapes (e.g., the Dust Bowl drought in the North American Great Plains). Interparticle forces make lifting small particles difficult and, as a result, suspended particles are typically entrained through secondary processes such as collisions and dust devils (*Bagnold,* 1941; *Nishimura and Hunt,* 2000).

5.2.3. Aeolian deposits and bedforms. Aeolian deposits include fine-grained material such as loess, desert pavement, sand sheets, dune fields, and sand seas or ergs. Loess, which are deposits of wind-blown silt-sized particles, cover up to ~10% of Earth's surface and are the closest analog to the aeolian dust deposits found at all elevations on Mars (*O'Hara-Dhand et al.,* 2010). Deposition of silt and clay-sized material plays a major role in the inflation of desert pavement surfaces. Desert pavement, which is common in Earth's arid regions and similar to surfaces observed at Gusev Crater on Mars, consist of a lag deposit of gravel or larger clasts that armor underlying fine-grained material against deflation. Fine-grained material may be incorporated into the underlying mantle through wetting-drying cycles, freeze-thaw cycles, and/or bioturbation (*Pelletier et al.,* 2007). Sand seas, or ergs (the names are used interchangeably), are areas of wind-lain sand deposits that cover a minimum of 125 km^2 (*Fryberger and Alhbrandt,* 1979). Smaller regions of sand cover are termed dune fields or, if they are relatively dune free, sand sheets.

Aeolian bedforms are known to occur on Earth, Mars, Venus, and Titan (Fig. 13) and emerge from grain interactions and self-organization regardless of differences in the fundamental variables affecting sediment transport such as gravity, fluid density, and particle composition (*Anderson,* 1990; *Werner and Kocurek,* 1999; *Kocurek et al.,* 2010). Remarkably, individual dune patterns characteristics (e.g., length and spacing) appear to be independent of these environmental parameters and are self-similar over a wide range of scales (Fig. 14) (*Hayes et al.,* 2012). Dune fields that are not in equilibrium with respect to wind regime, sediment supply, or sediment availability have been shown to have pattern variables that are distinct from those that are in equilibrium (e.g., *Ewing et al.,* 2010). For a given crest spacing, dune fields that have significantly shorter average crest lengths are either still evolving toward equilibrium or have been modified by a change in climatic or geomorphic conditions, resulting in crestlines that are either truncated or broken up by a new generation of dunes (*Beveridge et al.,* 2006; *Derickson et al.,* 2007; *Ewing et al.,* 2010).

Similar to fluvial bedforms, aeolian dunes occur at different scales as part of a hierarchy of bedforms that comprise, in order of increasing size, wind ripples (spacing 0.1–1 m), simple dunes (either isolated or superimposed on top of larger bedforms), compound or complex dunes, and draa (spacing greater than ~500 m). Dune morphology responds to both wind regime (magnitude and orientation) and sediment supply. The main morphologic dune classifications are crescentic (barchans and transverse), crescentic ridges (laterally linked crescentic dunes), linear, star, and parabolic (*McKee,* 1979). Barchan dunes (Fig. 13a) typically occur in areas of limited sediment supply, align their ridges perpendicular to their transport direction, and coalesce laterally to form crescentic ridges as sand supply increases. Linear dunes (Figs. 13b,d) are characterized by their long sinuous crestlines, parallel orientation, and regular spacing. They form in areas of a bimodal wind regime, although linear dunes can also form in a unimodal wind regime if the sediment is highly cohesive (*Rubin and Hesp,* 2009). Vast sand seas of linear dunes, presumably composed of dark organic sediment, are found within 30° of Titan's equator (*Lorenz et al.,* 2006). Star dunes have multiple crestlines (Fig. 13b) and form in multidirectional or complex wind regimes. The largest dunes observed on Earth are examples of star dunes and, in some cases, linear dunes are observed to transition into star dunes when sediment availability is reduced. Crescentic, linear, and star dunes have been observed on Earth, Mars, and Titan. Dunes orient their crestlines such that they are as perpendicular as possible to all dune-forming winds [i.e., the concept of maximum gross bedform normal transport described by *Rubin and Hunter* (1987)] and, in the case of large linear dunes, can take hundreds of thousands of years to react to changes in the wind regime. On the other hand, smaller bedforms, such as wind ripples and isolated simple dunes, can reorient within much short time periods (hours to hundreds of years). As a result of these characteristics, dunes, especially multiscale dune fields, represent unique and robust records of both past and present climatic conditions on any planetary body (e.g., *Ewing et al.,* 2010).

6. SEDIMENT DEPOSITION AND STRATIGRAPHIC RECORD

6.1. Earth

On Earth, source-to-sink systems are part of the rock cycle driven by plate tectonics, and regional subsidence in large sedimentary basins is what creates and preserves the stratigraphic record. Uplift and denudation of mountains generate large volumes of sediment that are transported to oceans almost entirely by fluvial processes. Deposition typically occurs at numerous intermediate points in sediment routing pathways, in addition to significant accumulation in major basins that act as terminal sinks (Fig. 1). In each case, deposition is due to a divergence in the flux of water due to local conditions including, for example, overbank flooding of streams, flow expansion where channelized flows enter bodies of standing water, or decrease in channel slope.

Examples of intermediate sediment repositories include soils of mountainous regions, where weathering occurs and sediment particles are generated. Once captured by streams,

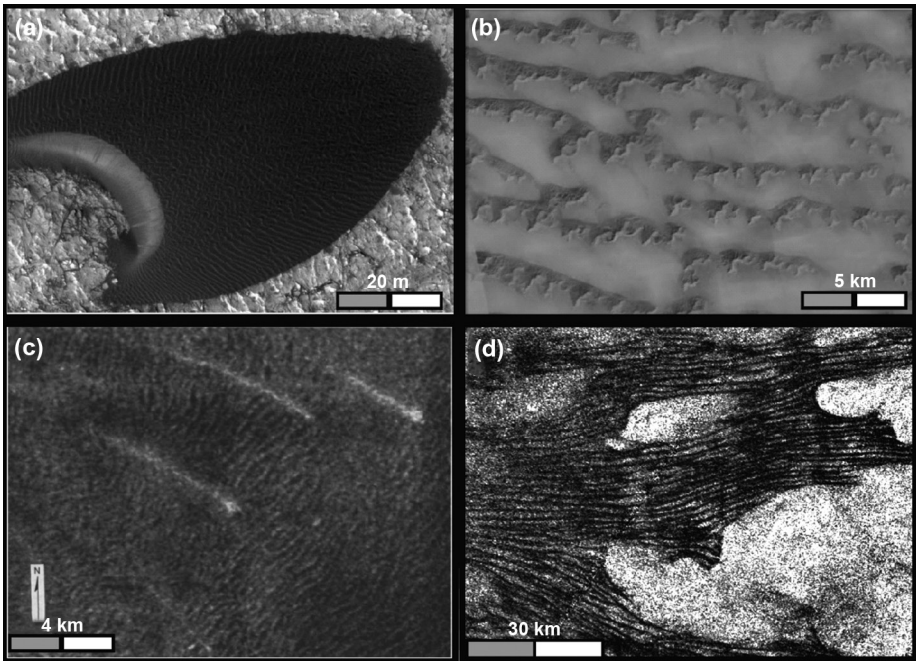

Fig. 13. Aeolian bedforms on Mars, Earth, Venus, and Titan. **(a)** Barchan dune with superimposed wind ripples in Nili Patera, Mars (*Ewing et al.,* 2010). **(b)** Linear and star dunes in Rub' al Khali, Oman, Earth. **(c)** Fortuna-Meshkenet dune field on Venus. Note that the wind streaks suggest a northwest wind direction, while the dunes are oriented between east-west and northeast-southwest (*Greeley et al.,* 1992). **(d)** Linear dunes diverted around topography in the Belet dune field on Titan.

temporary deposition may occur in abandoned channels or floodplains. In arid climates sediments may be transported from dry river beds to form sheets of windblown sand and silt. However, most sediments that are produced on Earth end up being deposited in ocean basins — the terminal sink (Fig. 1). This might include deltas, continental margins, or submarine fans at the base of the continental rise. There they will reside for tens to hundreds of millions of years before those sediments are recycled back into the sedimentary system after uplift due to plate convergence (e.g., continental collision) or into the mantle during subduction of lithospheric plates. Accordingly, uplift of previously deposited sediments and sedimentary rocks will result in their erosion and conversion back into sedimentary particles. In this regard, Earth is different from all other planets because sediment transport pathways are part of a longer-term tectonic cycle. On Venus, Mars, and Titan sediment transport is driven, at least in large part, by topographic gradients generated through other processes such as impacts and volcanism. Earth also differs in that the overwhelming majority of sediments were deposited in oceans and, to a lesser degree, streams. Eolian and ice-related deposits are relatively rare.

Earth's stratigraphic record preserves evidence of these processes at earlier times in its history. Sedimentary basins are sites of preferentially thick accumulation of sediments, where they become lithified through cementation and filling of initial pore space to form sedimentary rocks. Sedimentary basins on Earth are created by tectonic subsidence driven by two geodynamic processes: thinning due to stretching of the lithosphere, or dynamic depression of the lithosphere due to tectonic loading during mountain building. In either case broad depressions are created into which sediments are transported, creating accumulations that can range up to 20 km in thickness, but generally are on the order of 5–10 km. Significantly, thickness is proportional to the amount of tectonic subsidence — this is not something that necessarily holds true for either Mars or Titan.

Sedimentary strata that formed in these intermediate and terminal sinks can preserve signals of past climates, which can be revealed once the influence of tectonics and intrinsic dynamics in the transport system (e.g., *Jerolmack and Paola,* 2010) have been removed. In some cases climate variability is expressed as high-frequency variations in stratigraphic thickness, which may map back to changes in sea level and ice volume (*Goldhammer et al.,* 1987). Changes in sedimentary rock composition may also relate to climate change (*Warren,* 2010); in some rare cases dramatic shifts may be inferred (*Hoffman et al.,* 1998). But in many cases ancient changes in climate are recovered from variations in other proxies that are embedded within the stratigraphic record, which serves as a sort of "carrier signal." Sediments

that accumulate as a result of (bio)chemical precipitation show this best. For example, carbonate strata may show variability in silicate or oxide mineral content, organic carbon concentration, or oxygen isotope ratios, to name just a few. While over the past million years of Earth history the best climate records may be found in ice cores, or cave deposits such as stalagmites, only sediments and sedimentary rocks can preserve evidence of Earth's earlier climate history — extending back ~3.5 b.y. (Fig. 3).

6.2. Mars

In contrast to Earth, Mars has never had plate tectonics that affected the cycling of materials, nor has it developed large sedimentary basins that actively subsided during sediment accumulation (*McLennan and Grotzinger,* 2008). In the absence of plate tectonics, it appears that the flux of sediment has declined over time (*Grotzinger et al.,* 2011; *Grotzinger and Milliken,* 2012). Early on, primary sediments may have consisted mostly of impact- and volcanic-generated particles that could have been transported by fluvial and aeolian processes. Chemical weathering of fragmented bedrock in the presence of near-neutral pH fluids would have generated clays and rare carbonates; weathering under more acidic conditions generated dissolved salts that precipitated as sulfates, halides, and rare carbonates (*McLennan et al.,* 2005; *Ehlmann et al.,* 2011; *Morris et al.,* 2010; *Milliken and Bish,* 2010). Over time, Mars is regarded to have undergone an evolution from more neutral pH weathering, to more acidic weathering, to eventual desiccation (*Bibring et al.,* 2006). As the flux of impactors and volcanism declined, and the planet lost its hydrologic cycle, the formation of sedimentary rocks also declined. Today Mars appears to be in a net state of erosion and outcrops of sedimentary rocks are exposed as a result of wind-driven denudation.

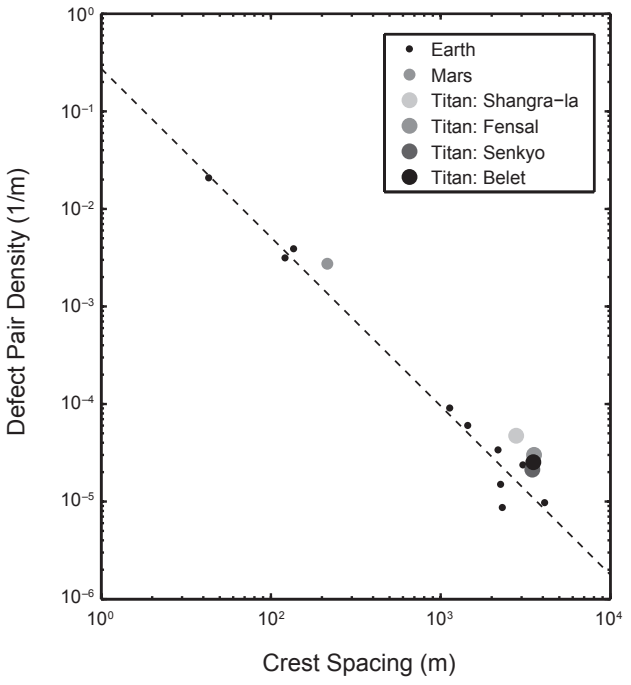

Fig. 14. Logarithmic plot of dune crest spacing vs. defect density on Earth, Mars, and Titan. Defect density is the inverse of the average dune crest length. Note that the data points follow a similar power law relationship, irrespective of environmental conditions. Dune fields that do not follow this relationship are observed to be out of equilibrium with either the local wind regime or sediment availability.

Nevertheless, some sedimentary deposits were formed and deposited locally, whereas other, more substantial, deposits accumulated as vast sheets that can be correlated for at least hundreds of kilometers (*Grotzinger and Milliken,* 2012). Local deposits were formed in alluvial fan, deltaic, sublacustrine fan, and lacustrine environments, in addition to canyon/valley-filling fluvial deposits of likely catastrophic origin. These former deposits suggest a more gradualistic view of sedimentation on Mars, perhaps even involving meteoric precipitation (e.g., *Mangold et al.,* 2004; *Hynek et al.,* 2010), which complements the Viking-era view of Mars that highlighted great catastrophic floods of more regional extent that were formed during sudden outbursts of groundwater. Regionally extensive sedimentary deposits have less obvious origins, but significant quantities of hydrated sulfate minerals suggest that some of these may have formed as lacustrine evaporites, particularly in the Valles Marineris canyon/chasma network of basins. Others may have involved aeolian reworking of previously deposited sulfates, or perhaps aqueous (groundwater) alteration of previously deposited basaltic sediments (*Grotzinger et al.,* 2005; *McLennan et al.,* 2005). The Burns formation at Meridiani Planum is the type example of this sort of deposit having been studied in detail by the Opportunity rover at multiple locations. At every locality visited it features largely or entirely aeolian traction deposits representing ancient sand dunes and draas, but punctuated by brief episodes of fluvial transport (*Grotzinger et al.,* 2005, 2006; *Metz et al.,* 2009; *Hayes et al.,* 2011b; *Edgar et al.,* 2012). Only recently has evidence been presented for a possible lacustrine mudstone, significantly different in grain size and diagenesis from other facies of the Burns formation (*Edgar,* 2013). The Burns formation has been alternatively interpreted to represent an impact or volcanic base surge deposit (*Knauth et al.,* 2005; *McCollom and Hynek,* 2005); however, this model is inconsistent with available data that support aeolian/fluvial interpretations (*McLennan and Grotzinger,* 2008; *Fralick et al.,* 2012).

Another major type of regionally extensive sedimentary deposit occurs as meter-scale stratification with highly rhythmic organization (Fig. 3b) and is well developed over much of Terra Arabia. The significant lateral continuity of relatively thin beds, their distribution over broadly defined highs as well as lows, and the lack of strong spectral absorption features suggests these rocks may be "duststones," formed by settling of fine particulates from the ancient

martian atmosphere (*Bridges and Muhs,* 2012; *Grotzinger and Milliken,* 2012). Sedimentation may have been driven by climate cycles in the Milankovitch bands (*Lewis et al.,* 2008). The most ancient sedimentary deposits on Mars may be dominated by stacked impact-generated debris sheets, similar to the Moon, and possibly including impact melt sheets.

In the past decade it has become clear that Mars has sediment sources and sinks distributed at both local and regional scale (see review in *Grotzinger and Milliken,* 2012). One of the longest largest source-to-sink systems on Mars has its source in the Argyre region and extends to the northern lowlands, inferred to be the terminal sink. The total length of the outflow system, from where Uzboi Vallis begins at the rim of Argyre impact basin to where the outflow system discharges onto the northern plains at Chryse Planitia, is over 4000 km. It is hypothesized that fine-grained sediments transported through this system accumulated along the fringe of the northern lowlands. A series of valleys and basins, known as the Uzboi-Ladon-Morova network, link Argyre with the northern lowlands and trapped sediments in alluvial and lacustrine environments along the way to the northern lowlands (Fig. 15). The basins along this network are interpreted to once have been lakes, created when large impacts blocked drainage networks (*Grant and Wilson,* 2011). These impact basins are regarded as significant local sinks for sediments, including clay minerals (*Milliken and Bish,* 2010). The Ladon basin is the largest potential lake basin (Fig. 15b), although others are also developed, including the craters Holden and Eberswalde (Fig. 15c). Clay-bearing strata of possible lacustrine origin are preserved in the Ladon basin (Fig. 15d) and the Eberswalde-Holden Craters (Figs. 15a,b).

An enduring and controversial hypothesis asserts that the northern lowlands of Mars may represent a terminal sediment sink of a scale comparable to the ocean basins on Earth; the flattest surface in the solar system may reflect sedimentation at the bottom of a vanished ocean basin on Mars (*Aharonson et al.,* 1998). On the other hand, this very flat surface could owe its origin to accumulation of atmospheric dust over billions of years, in a manner perhaps similar to what has been suggested for the duststones of Terra Arabia (*Bridges and Muhs,* 2012; *Grotzinger and Milliken,* 2012). Other suggestions include lacustrine and lava flow deposits on the northern plains. In any case, the low-lying northern plains would still be a terminal sediment sink involving settling of suspended sediment from a fluid, either liquid water or air. Furthermore, in these scenarios, it is likely that the terminal sink represented by the northern lowlands is in part filled — at least at its margins — with sediments derived from the Argyre-to-Chryse fluvial system.

6.3. Titan

The evidence for extensive atmospheric precipitation, standing bodies of liquid, and channelized flow makes Titan the only extraterrestrial body in the solar system with an active hydrologic cycle. Similar to Mars, Titan has never been subject to plate tectonics and does not, at least currently, have a surface ocean to act as terminal sediment sink. Unlike Mars and Venus, Titan is subject to active pluvial, fluvial, and lacustrine processes. Titan's methane-based hydrologic cycle drives a source-to-sink sediment transport system that generates morphologic features, including dunes, rivers, and lakes, that are strikingly similar to morphologies found on Earth and Mars (Figs. 2e,f). Unlike Earth and Mars, however, there is no obvious recycling method for these deposits. Unfortunately, the low resolution at which we have observed Titan's surface (~300 m) makes it difficult to study any stratigraphic record deposited by this system.

Sediment on Titan can consist of both water-ice and organic particulates. Sediments can be generated through fluvial and aeolian erosion of bedrock, or by impact and possible cryovolcanic processes that generate sediment that is then relocated through fluvial and aeolian transport (section 3). The anomalously high radar backscatter of a subset of the fluvial valleys observed by the Cassini RADAR (predominantly those found at equatorial latitudes) has been interpreted as resulting from the deposition of water-ice cobbles that act as semitransparent Mie scatterers (*Le Gall et al.,* 2010), and the low backscatter and infrared signature of Titan's dunes suggests transport and deposition of sand-sized organic sediment; it is possible that these deposits form stratigraphic units, although their extent and thickness are not currently known. Organic sediment consists of higher-order hydrocarbons (C_xH_y) and nitriles ($C_xH_yN_z$) that are generated through methane photolysis in Titan's upper atmosphere (*Lorenz and Lunine,* 1996). This material settles through the atmosphere to coat the surface in a veneer of organic material. The thickness of this organic layer is dependent on both the specific photolysis pathways active in the atmosphere, which determine the flux of sediment, and the persistence of methane, which determines the timescales for production. At its present rate, photolysis would deplete the atmospheric methane content in ~26 m.y. (*Yung et al.*, 1984). Without methane, which is Titan's primary greenhouse gas, the nitrogen-based atmosphere would partially collapse and likely shut down active sediment transport and deposition (*Lorenz et al.,* 1997). The rate and nature (episodic vs. continuous) of methane outgassing from Titan's interior (e.g., *Tobie et al.,* 2006; *Nelson et al.,* 2009; *Moore and Pappalardo,* 2011; *Choukroun and Sotin,* 2012) will control source terms in the sediment transport system.

The largest sedimentary repositories on Titan are vast equatorial dune fields found within 30° of the equator. Dunes encompass ~12.5% of Titan's surface (*Le Gall et al.,* 2012). If the dunes are composed of organics, they represent the largest reservoir of hydrocarbon on Titan, estimated at 250,000 km^3, assuming dunes heights of 100 m (*Le Gall et al.,* 2012). However, this volume is still smaller than most estimates of photolysis production, assuming a continuous supply of methane, which suggests the presence of an additional unseen hydrocarbon reservoir, overestimation

of photolysis production, or discontinuous (i.e., episodic) production (*Lorenz et al.,* 2008). Unseen hydrocarbon reservoirs could include a subsurface ocean stored in the porous upper crust, large crustal clathrate reservoirs, or the incorporation of thick sand sheet deposits in the amorphous plains that dominate the midlatitudes (*Lopes et al.,* 2010). The detection of radiogenic ^{40}Ar suggests geologically recent interaction between Titan's interior and atmosphere (*Niemann et al.,* 2005) and has motivated the development of episodic methane outgassing models that predict methane-free periods in Titan's climatic history (e.g., *Tobie et al.,* 2006).

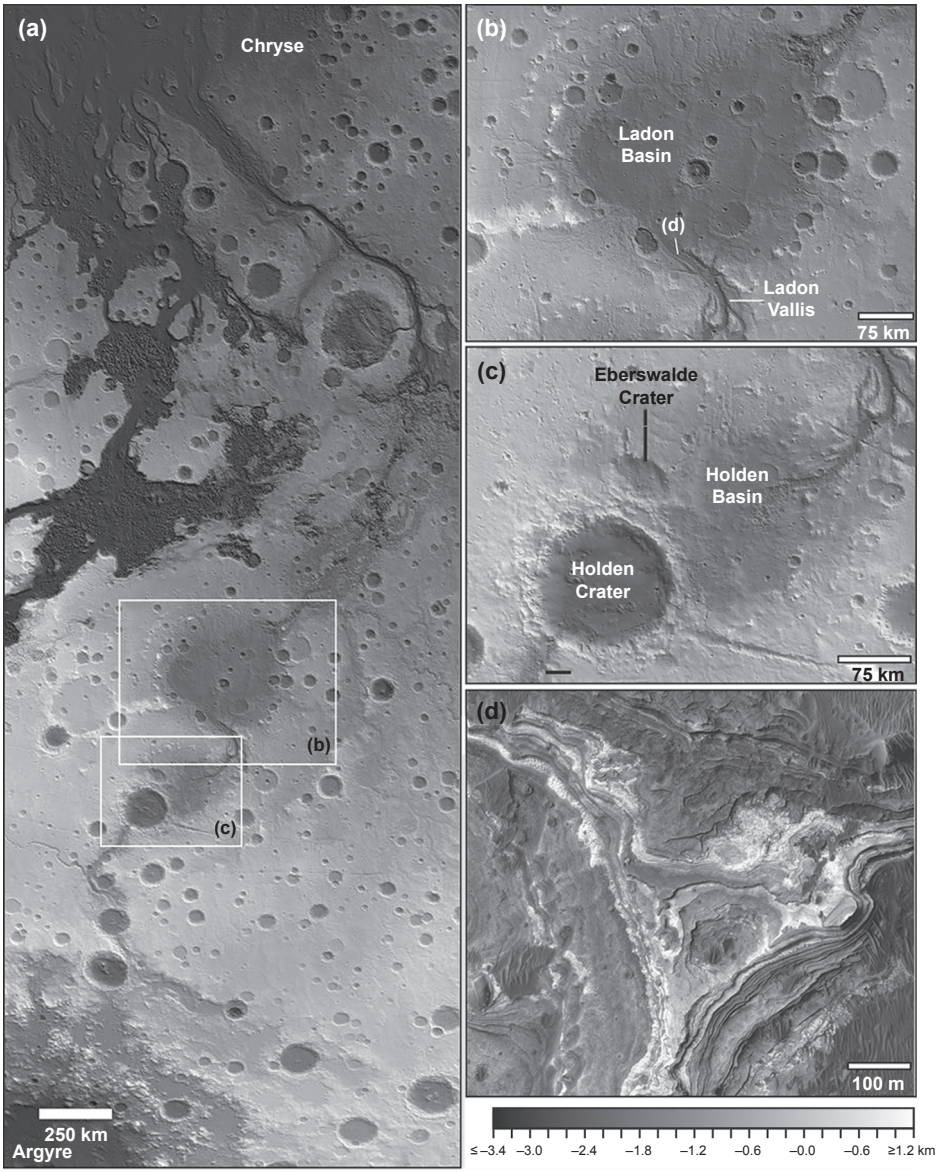

Fig. 15. The Uzboi-Ladon-Morava (ULM) source-to-sink system. **(a)** MOLA elevation shows the low elevation of the ULM system relative to the surrounding ancient highlands. The ULM system was once throughgoing from the northern rim of the Argyre impact basin to Chryse Planitia at the edge of the northern lowlands, but it was blocked at one point by the formation of Holden Crater [see **(c)**]. Much of the channel system exhibits evidence for sedimentary fill and multiple episodes of incision. **(b)** Close-up of the ancient Ladon Basin, which has been filled with sediment of an unknown thickness; numerous fluvial features are found along the heavily degraded rim and wall. **(c)** Close-up of Eberswalde Crater (see also Fig. 2d), Holden Crater, and the more ancient Holden Basin; breach of Uzboi Vallis into Holden Crater is visible in the southwest portion of the image; note that the formation of Holden Crater blocked water flow through the larger ULM system. **(d)** Close-up of finely stratified sedimentary outcrops exposed in a terrace in Ladon Vallis where it enters Ladon Basin along the southern rim; location marked by "**(d)**" in **(b)**; HiRISE image PSP_006637_1590. After *Grotzinger and Milliken* (2012).

In the polar regions, lakebeds are the primary sediment sinks. The presence of these features, which include both small (lakes) and large (seas or mare) standing bodies of liquid as well as empty depressions (empty lakes), imply mechanisms that can generate topographic lows at multiple scales (*Hayes et al.,* 2008). These processes can include, but are certainly not limited to, tectonic subsidence and sediment loading at large scales, and dissolution or solution processes at all scales. Impact and volcanic processes are also possible, but are generally not considered the primary mechanism for basin formation (see the recent review by *Aharonson et al.,* 2013).

Lacustrine features are observed both connected to and independent of regional and local drainage networks. The largest lakes, or seas, in the north, consisting of Ligeia, Kraken, and Punga Mare, have shorelines that include shallow bays with drowned river valleys (Figs. 16a,b). Such drowned valleys indicate that once well-drained upland landscapes became swamped by rising fluid levels where sedimentation did not keep pace with the rising relative base level. The absence of sedimentary deposits at the terminus of these valleys provides further evidence for relatively rapid increases in liquid level. At Ligeia Mare, nearby fluvial systems include a drainage network that runs parallel to the sea shoreline (Fig. 16a). As the modern slope is perpendicular to the shoreline, such an orientation may suggest a large-scale, and apparently nonuniform, down-dropping of topography associated with sea formation. As base level rose, the shores of Ligeia Mare encroached on this network, and in some cases shoreline retreat appears to be erasing topography as evidenced by the abrupt termination of large river valleys at the shoreline.

While the areal abundance of lakes in the south polar region is ~25 times smaller than in the north, albedo-dark regions observed in the lowest elevations of the south may represent preserved paleoshorelines of past seas that could have once encompassed areas comparable to their northern counterparts (*Hayes et al.,* 2011a). The asymmetric distribution of filled lakes between Titan's north and south polar regions has been attributed to the 25% increase in peak solar insolation between northern and southern summer, arising from Titan's current orbital configuration (*Schneider et al.,* 2012). Analogous to Croll-Milankovich cycles on Earth, the orbital parameters that determine Titan's insolation pattern cycle on timescales of tens of thousands of years (*Aharonson et al.,* 2009), potentially driving variations in polar sediment transport and deposition.

In addition to the dunes and mare, smaller-scale depositional morphologies have also been observed on Titan. RADAR-bright alluvial fans (e.g., Elvigar Flumina) (*Lorenz et al.,* 2008), lobate structures interpreted as deltas at Ontario Lacus (*Wall et al.,* 2010), isolated lacustrine environments (*Hayes et al.,* 2008), and other fluvial deposits (*Burr et al.,* 2013) have been documented. These deposits appear to be associated with local deposition and may or may not represent terminal sediment sinks. Empty lake basins are a few hundred meters deep and have significantly different microwave scattering characteristics than surrounding terrain (*Hayes et al.,* 2008). These empty lakebeds are also

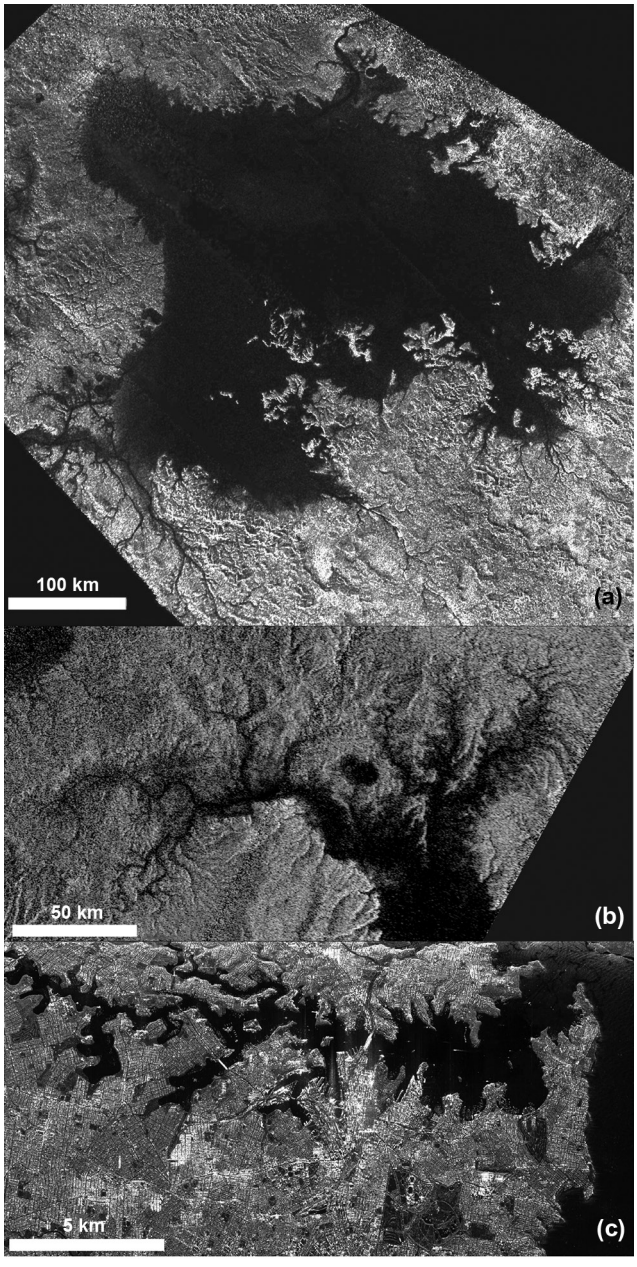

Fig. 16. **(a)** Polar stereographic mosaic of Titan's Ligeia Mare using Synthetic Aperture Radar (SAR) data acquired between February 2006 and April 2007. The crenulated shoreline morphology and shallow bays are characteristic of drowned topography. North is approximately up. **(b)**,**(c)** Examples of drowned river valleys on Titan [**(b)**] and Earth [**(c)**]; **(b)** Ku-Band SAR image of a drowned-river valley on Titan acquired in April 2007, centered at (76°N, 80°E) near the westernmost shores of Kraken Mare; **(c)** C-Band AIRSAR image of Georges River, a drowned river valley located in Sydney, Australia. AIRSAR data was obtained from the Alaska Satellite Facility (*www.asf.alaska.edu*).

observed to be bright at 5 μm, which *Barnes et al.* (2011) interpreted as evidence of organic evaporite deposits. The equatorial basins Hotei and Tui Regio, which are similarly bright at 5 μm, have also been identified as candidate paleolakes partially filled in by evaporites (*Moore and Howard,* 2010). Lobate flow-like morphologies observed in both regions, however, have been used to suggest a cryovolcanic origin for these deposits (e.g., *Lopes et al.,* 2013). Regardless, it is unclear how these precipitants could be transported out of the closed basins in which they are observed, suggesting that they may act as terminal sediment sinks. Spectrally distinct rings observed around Ontario Lacus further suggest that evaporites are deposited on Titan (*Barnes et al.,* 2011).

Titan also may have intermediate sediment repositories analogous to mountainous soils found on Earth. *Turtle et al.* (2011) observed a darkening of ~500,000 km^2 of terrain following a large equatorial cloudburst in September 2010. This was interpreted as evidence of surface wetting and/or ponding from a precipitation event. In the year following the storm event, the region returned to its original albedo, with the exception of a specific morphologic feature — VIMS Equatorial Bright Terrain (*Soderblom et al.,* 2007) — which appeared to brighten prior to returning to their original spectrum (*Barnes et al.,* 2013). This brightening was interpreted as evidence for volatile precipitation (*Barnes et al.,* 2013).

6.4. Venus

The surface of Venus was entirely resurfaced by volcanism and related processes at about 750 Ma in a process that probably took on the order of <100 m.y. (see *Taylor and McLennan,* 2009, for a recent review). Accordingly, any evidence for whether or not Venus ever had an ancient stratigraphic record of sedimentary deposits is permanently obscured. There is no evidence to suggest a more recent (<750 Ma) stratigraphic record apart from the limited occurrence of surficial aeolian deposits.

7. CONCLUSIONS

1. Interactions between atmospheric and geologic processes influence the morphology and composition of planetary surfaces, and over the course of geologic time determine the historical evolution of the planet's surface environments including climate. The flow of currents of air, liquid water, and ice in turn transport sediments from sites of weathering and erosion where they are formed, to sites of deposition where they are stored, to create a stratigraphic record of layered sediments and sedimentary rocks.

2. This transfer of sediment and solute mass from source to sink plays a key role in the cycling of elements, water, and fractionation of biogeochemically important isotopes, as well as the formation of soils, groundwater reservoirs, masses of sediment, and the composition of the atmosphere. Models based on conservation of mass and simple transport laws show how the ancient rock record may preserve evidence of surface processes, including the influence of climate.

3. The form, intensity, and duration of weathering vary greatly and are influenced by surface mineralogy (e.g., basalt vs. granite vs. ice) and the presence, extent, and composition of atmosphere (e.g., S-cycle vs. C-cycle) and hydrosphere, which in turn are controlled by climate, the nature of tectonics (e.g., influencing topography), and impact history.

4. Chemical and physical weathering, which initiates reequilibration of minerals formed at high P-T to those stable under surface conditions, generates solute-bearing solutions (including brines) and promotes formation of sedimentary particles. Weathering influences all planetary surfaces including those on Earth, Mars, Venus, and Titan, occurring even on planetary bodies that lack atmospheres (albeit at very low rates).

5. Weathering on Earth is a result of chemical, physical, and biological processes operating on silica-rich continental crust. Mars differs in the apparent absence of biological influences, as well as the preponderance of basaltic crust. After Noachian time, weathering on Mars was likely dominated by low-pH and possibly briny fluids. Venus likely experiences limited but very heterogeneous weathering due to lack of surface water but extremes in atmospheric temperature, pressure, and density. There is no evidence for fluvial processes and the entire planet was resurfaced ~1 b.y. ago. Titan shows only trivial temperature variation at its surface, which limits physical weathering. Chemical weathering of water-ice substrates are likely caused by interactions with alkane-rich fluids. Sediments also are contributed by the novel mechanism of methane photolysis in the atmosphere, and aggregate to form particles at the surface.

6. For low-gradient river systems and aeolian transport we have robust semi-empirical equations for the inception of sediment motion, sediment fluxes, and equilibrium bed states. These formulae have been thoroughly tested such that their application to planetary bodies with different gravitational acceleration, particle densities, fluid densities, and fluid viscosities is well founded. For many cases (e.g., channelized fluid flow and transport of coarse particles) fluid deformation is governed by turbulence and molecular viscosity ceases to play a role in transport dynamics. These equations can be used in combination with observations of active sediment transport and bed states (e.g., existence of dunes), or records of past processes preserved within the sedimentary strata, to reconstruct wind and river flow rates, which in turn can constrain atmospheric processes.

7. Such robust, quantitative theory is lacking for a number of first-order processes in sediment production and transport including rock abrasion by rivers and wind, plucking of jointed rock, waterfall and knickpoint retreat, groundwater seepage erosion, and sediment transport and equilibrium bed states in steep mountain channels. For these processes experiments and field observations on Earth are needed to build a quantitative understanding that can be applied to other planets.

8. Aeolian sediment transport and deposition is the only sedimentologically important process that is shared in common by Earth, Mars, Venus, and Titan. The threshold for grain entrainment by the wind is significantly lower for Venus and Titan as compared to Earth and Mars. Earth and Titan are the wettest planets and so have correspondingly small volumes of aeolian sediment as compared to Mars, which has vast deposits of both modern and ancient wind-blown deposits. Venus shows very limited aeolian deposits, perhaps because of the low production rate of saltatable sediment particles, which in turn limits supply and availability.

9. Processes that operate at planetary surfaces have the potential to record a history of their evolution in the form of sedimentary rocks. Earth's record is strongly influenced by plate tectonics and biological processes, and deposition occurs predominantly in marine settings, and with extensive recycling.

10. Mars preserves a perhaps simpler but surprisingly vast record, likely dominated by aeolian and, earlier on, impact processes; almost all sediments represent primary deposits with very limited recycling. Interaction with water was more extensive prior to ~ 3 b.y. ago, and even then it is possible that transport and alteration occurred dominantly in the presence of brines, with limited water/rock interaction. The sedimentary rock record bears evidence for global transitions from clay, to sulfate, to anhydrous ion oxide-bearing sediments.

11. Titan does not have an observed stratigraphic record, yet patterns of sedimentation involving water-ice and organic particles suggest one may exist. Broad alluvial valleys are covered with bimodally sized sediments suggesting that deposits underlie these surfaces. Organic sediment generated through methane photolysis in the upper atmosphere may coat the surface of Titan, and its accumulation rate depends on methane degassing from the planet's interior. This organic sediment is reworked to form aeolian bedforms. Lakebeds in polar regions may represent significant sinks for Titan's sediments. The current undersupply of sediment relative to rising liquid base levels in the north polar region results in flooded drainage networks; however, the south polar basins may preserve paleo-shorelines and sedimentary deposits.

Acknowledgments. Funding was provided by the NASA Astrobiology Institute and Mars Science Laboratory Project to J.P.G., and by the Miller Institute for Basic Research in Science to A.G.H. S.M.M. was supported by NASA Mars Data Analysis and Mars Fundamental Research grants. J. Griffes and K. Stack helped with construction of Figs. 1, 2, and 4. Thanks to D. Burr, L. Sklar, and two anonymous reviewers for comments on an earlier version of this chapter.

REFERENCES

Aharonson O., Zuber M. T., Neumann G. A., and Head J. W. (1998) Mars: Northern hemisphere slopes and slope distributions. *Geophys. Res. Lett., 25,* 4413–4416.

Aharonson O., Hayes A. G., Lunine J., Lorenz R., Allison M., and Elachi C. (2009) An asymmetric distribution of lakes on Titan as a possible consequence of orbital forcing. *Nature Geosci., 2,* 851–854.

Aharonson O., Hayes A. G., Lopes R. M. C., Lucas A., Hayne P., and Perron T. (2013) Titan's surface geology. In *Titan: Surface, Atmosphere, and Magnetosphere* (I. Mueller-Wodarg, ed.), Cambridge Univ., Cambridge. ISBN 13:978052119926.

Allen P. A. (2008) From landscapes into geological history. *Nature, 105,* 274–276.

Almeida M. P., Parteli E. J. R., Andrade J. S., and Herrmann H. J. (2008) Giant saltation on Mars. *Proc. Natl. Acad. Sci., 105,* 6222–6226.

Amundson R., Richter D. D., Humphyreys G. S., Jobbagy E. C., and Gaillardet J. (2007) Coupling between biota and Earth materials in the critical zone. *Elements, 3,* 327–332.

Anderson R. S. (1986) Erosion profiles due to particles entrained by wind: Application of an eolian sediment-transport model. *Geol. Soc. Am. Bull., 97,* 1270–1278.

Anderson R. S. (1990) Eolian ripples as examples of self-organization in geomorphological systems. *Earth Sci. Rev., 29,* 77–96.

Anderson R. S. and Haff P. K. (1988) Simulation of eolian saltation. *Science, 241,* 820–823.

Anderson S. P., von Blanckenburg F., and White A. F. (2007) Physical and chemical controls on the critical zone. *Elements, 3,* 315–319.

Bagnold R. A. (1941) *The Physics of Blown Sand and Desert Dunes*. Methuen, London. 256 pp.

Bagnold R. A. (1966) *An Approach to the Sediment Transport Problem from General Physics*. U.S. Geological Survey, Washington, DC. 37 pp.

Baker V. R. (1982) *The Channels of Mars*. Univ. of Texas, Austin. 198 pp.

Baker V. R., Komatsu G., Parker T. J., Gulick V. C., Kargel J. S., and Lewis J. S. (1992) Channels and valleys on Venus: Preliminary analysis of Magellan data. *J. Geophys. Res., 97,* 13421–13444.

Barnes J. W., Bow J., Schwartz J., Brown R. H., Soderblom J., Hayes A. G., Le Mouelic S., Rodriguez S., Sotin C., Jaumann R., Stephan K., Soderblom L. A., Clark R. N., Buratti B. J., Baines K. H., and Nicholson P. D. (2011) Organic sedimentary deposits in Titan's dry lake beds. *Icarus, 216(1),* 136–140.

Barnes J., Burrati B., Turtle E., Bow J., Dalba P., Perry J., Brown R., Rodriguez S., Le Mouelic S., Baines K., Sotin C., Lorenz R., Malaska M., McCord T., Clark R., Jaumann R., Hayne P., Nicholson P., Soderblom J., and Soderblom L. (2013) Precipitation-induced surface brightenings seen on Titan by Cassini VIMS and ISS. *Planetary Sci., 2:1.*

Basilevsky A. T. and Head J. W. (1993) The surface of Venus. *Rep. Prog. Phys., 96,* 1699–1734.

Basilevsky A. T., Kuzmin R. O., Nikolaeva O. V., Pronin A. A., Ronca L. B., Avduevsky V. S., Uspensky G. R., Choremukhina Z. P., Semenchenko V. V., and Ladygin V. M. (1985) The surface of Venus as revealed by the Venera landings: Part II. *Geol. Soc. Am. Bull., 96,* 137–144.

Berner E. K., Berner R. A., and Moulton K. L. (2004) Plants and mineral weathering: Past and present. In *Treatise on Geochemistry, Vol. 5: Surface and Ground Water, Weathering , and Soils* (J. I. Drever, ed.), pp. 169–188. Elsevier-Pergamon, Oxford.

Berner R. A. (1995) Chemical weathering and its effect on atmospheric CO_2 and climate. *Rev. Mineral., 31,* 565–583.

Beveridge C., Kocurek R., Ewing R. C., Lancaster N., Morthekai

P., Singhvi A. K., and Mahan A. (2006) Development of spatially diverse and complex dune-field patterns: Gran Desierto Dune Field, Sonora, Mexico. *Sedimentology, 53,* 1391–1409.

Bibring J.-P., Langevin Y., Mustard J. F., Poulet F., Arvidson R., Gendrin A., Gondet B., Mangold N., Pinet P., Forget F., and the OMEGA Team (2006) Global mineralogical and aqueous Mars history derived from OMEGA/Mars Express data. *Science, 312,* 400–404.

Bibring J.-P., Arvidson R. E., Gendrin A., Gondet B., Langevin Y., Le Mouelic S., Mangold N., Morris R. V., Mustard J. F., Poulet F., Quantin C., and Sotin C. (2007) Coupled ferric oxides and sulfates on the martian surface. *Science, 317,* 1206–1210.

Bourke M. C., Lancaster N., Fenton L. K., Parteli E. J. R., Zimbelman J. R., and Radebaugh J. (2010) Extraterrestrial dunes: An introduction to the special issue on planetary dune systems. *Geomorphology, 121,* 1–14.

Brantley S. L. and Chen Y. (1995) Chemical weathering rates of pyroxenes and amphiboles. *Rev. Mineral., 31,* 119–172.

Brantley S. L. and Lebedeva M. (2011) Learning to read the chemistry of regolith to understand the critical zone. *Annu. Rev. Earth Planet. Sci., 39,* 387–416.

Brantley S. L., Goldhaber M. B., and Ragnarsdottir K. V. (2007) Crossing disciplines and scales to understand the critical cone. *Elements, 3,* 307–314.

Bridges N. and Muhs D. (2012) Duststones on Mars: Source, transport, deposition and erosion. In *Sedimentary Geology of Mars* (J. Grotzinger and R. Milliken, eds.), pp. 169–182. SEPM Spec. Publ. 102, Society for Sedimentary Geology, Tulsa.

Bridges N. T., Ayoub F., Avouac J.-P., Leprince S., Lucas A., and Mattson S. (2012) Earth-like sand fluxes on Mars. *Nature, 485,* 339–342.

Brownlie W. R. (1983) Flow depth in sand-bed channels. *J. Hydraul. Eng.-ASCE, 109,* 959–990.

Burr D. M. (2010) Palaeoflood-generating mechanisms on Earth, Mars, and Titan. *Global Planet. Change, 70,* 5–13.

Burr D. M., McEwen A. S., and Sakimoto S. E. H. (2002) Recent aqueous floods from the Cerberus Fossae, Mars. *Geophys. Res. Lett., 29,* 1–4.

Burr D. M., Emery J. P., Lorenz R. D., Collins G. C., and Carling P. A. (2006) Sediment transport by liquid surficial flow: Application to Titan. *Icarus, 181,* 235–242.

Burr D. M., Perron J. T., Lamb M. P., Irwin R. P., Collins G., Howard A. D., Sklar L. S., Moore J. M., Ádámkovics M., Baker V., Drummond S. A., and Black B. A. (2013) Fluvial feature on Titan: Insights from morphology and modeling. *Geol. Soc. Am. Bull., B30612.1,* 1–23, DOI: 10.1130/B30612.1.

Burns R. G. (1993) Rates and mechanisms of chemical weathering of ferromagnesian silicate minerals on Mars. *Geochim. Cosmochim. Acta, 57,* 4555–4574.

Canfield D. E. (2004) The evolution of the Earth surface sulfur reservoir. *Am. J. Sci., 304,* 839–861.

Carr M. H. and Clow G. D. (1981) Martian channels and valleys — their characteristics, distribution, and age. *Icarus, 48,* 91–117.

Carr M. H. and Head J. W. (2010) Geologic history of Mars. *Earth Planet. Sci. Lett., 294,* 185–203.

Chabert J. and Chauvin J. L. (1963) Formation de Dunes et de Rides Dans Les Modeles Fluviaux. *Bull. Cen. Rech. Ess. Chatau, 4,* 31–51.

Chan M., Yonkee W. A., Netoff D. I., Seiler W. M., and Ford R. L. (2008) Polygonal cracks in bedrock on Earth and Mars: Implications for weathering. *Icarus, 194,* 65–71.

Chepil W. S. and Woodruff N. P. (1963) The physics of wind erosion and its control. *Adv. Agronomy, 15,* 211–302.

Chorover J., Kretzschmar R., Garcia-Pichel F., and Sparks D. L. (2007) Soil biogeochemical processes within the critical zone. *Elements, 3,* 321–326.

Choukroun M. and Sotin C. (2012) Is Titan's shape caused by its meteorology and carbon cycle? *Geophy. Res. Lett., 39,* L04201, DOI: 10.1029/2011GL050747,2012.

Chow V. T. (1959) *Open Channel Hydraulics*. McGraw Hill, New York. 680 pp.

Clark B. C. (1993) Geochemical components in martian soil. *Geochim. Cosmochim. Acta, 57,* 4575–4581.

Clark B. C., Baird A. K., Rose H. J., Toulmin P., Keil K., Castro A. J., Kelliher W. C., Rowe C. D., and Evans P. H. (1976) Inorganic analyses of martian surface samples at Viking landing sites. *Science, 194,* 1283–1288.

Clark B. C., Morris R. V., McLennan S. M., Gellert R., Jolliff B., Knoll A., Lowenstein T. K., and 19 colleagues (2005) Chemistry and mineralogy of outcrops at Meridiani Planum. *Earth Planet. Sci. Lett., 240,* 73–94.

Collins G. C. (2005) Relative rates of fluvial bedrock incision on Titan and Earth. *Geophys. Res. Lett., 32,* L22202, DOI: 10.1029/2005GL024551.

Craddock R. A. (2011) Aeolian processes on the terrestrial planets: Recent observations and future focus. *Progr. Phys. Geog., 36,* 110–124.

Curtis C. D. (1976) Stability of minerals in surface weathering reactions: A general thermochemical approach. *Earth Surf. Proc., 1,* 63–70.

Derickson D., Kocurek G., Ewing R. C., and Bristow C. (2007) Origin of a complex and spatially diverse dune-field pattern, Algodones, southeastern California. *Geomorphology, 99,* 186–204.

Deschamps F., Mousis O., Sanchez-Valle C., and Lunine J. I. (2010) The role of methanol in the crystallization of Titan's primordial ocean. *Astrophys. J., 724,* 887–894.

Dietrich W. E. (1982) Settling velocity of natural particles. *Water Res. Res., 18,* 1615–1626.

Dorn R. I. (2009) The role of climatic change in alluvial fan development. In *Geomorphology of Desert Environments* (A. D. Parsons and A. D. Abrahams, eds), pp. 723–742. Springer, London.

Easterbrook D. J. (1999) *Surface Processes and Landforms, 2nd edition.* Prentice-Hall, New Jersey. 546 pp.

Edgar L. A., Grotzinger J. P., Hayes A. G., Rubin D. M., Squyres S. W., Bell J. F., and Herkenhoff K. E. (2012) Stratigraphic architecture of bedrock reference section, Victoria Crater, Meridiani Planum, Mars. In *Sedimentary Geology of Mars* (J. Grotzinger and R. Milliken, eds.), pp. 195–210. SEPM Spec. Publ. 102, Society for Sedimentary Geology, Tulsa.

Edgar L. A. (2013) Identifying and interpreting stratification in sedimentary rocks on Mars: Insight from rover and orbital observations and terrestrial field analogs. Ph.D. thesis, California Institute of Technology, Pasadena.

Ehlmann B. L., Mustard J. F., Murchie S. L., Bibring J.-P., Meunier A., Fraeman A. A., and Langevin Y. (2011) Subsurface water and clay mineral formation during the early history of Mars. *Nature, 479,* 53–60.

Ewing R. C., Peyret A.-P. B., Kocurek G., and Bourke M. (2010) Dune field pattern formation and recent transporting winds in the Olympia Undae Dune Field, north polar region of Mars. *J. Geophys. Res.–Planets, 115,* 8005, DOI:

10.1029/2009JE003526.
Farmer A. M. (1993) The effects of dust on vegetation: A review. *Environ. Poll., 79,* 63–75.
Flemings P. B. and Grotzinger J. P. (1996) STRATA: Freeware for analyzing classic stratigraphic problems. *GSA Today, 6,* 1–7.
Florensky C. P., Ronca L. B., Basilevsky A. T., Burba G. A., Nikolaeva O. V., Pronin A. A., Trackhtman A. M., Volkov V. P., and Zasetsky V. V. (1977) The surface of Venus as revealed by Soviet Venera 9 and 10. *Geol. Soc. Am. Bull., 88,* 1537–1545.
Foley C. N., Economou T. E., Clayton R. N., Brückner J., Dreibus G., Rieder R., and Wänke H. (2008) Martian surface chemistry: APXS results from the Pathfinder landing site. In *The Martian Surface: Composition, Mineralogy, and Physical Properties* (J. F. Bell III, ed.), pp. 35–57. Cambridge Univ., Cambridge.
Fralick P., Grotzinger J., and Edgar L. (2012) Potential recognition of accretionary lapilli in distal impact deposits on Mars: A facies analog provided by the 1.85 Ga Sudbury impact deposit. In *Sedimentary Geology of Mars* (J. Grotzinger and R. Milliken, eds.), pp. 211–228. SEPM Spec. Publ. 102, Society for Sedimentary Geology, Tulsa.
Fryberger S. G. and Alhbrandt T. S. (1979) Mechanisms for the formation of eolian sand seas. *Z. Geomorphol., 23,* 440–460.
Gaffey M. J. (2010) Space weathering and the interpretation of asteroid reflectance spectra. *Icarus, 209,* 564–574.
Garcia M. H. (2007) *Sedimentation Engineering: Process, Measurement, Modeling, and Practice*. American Society of Civil Engineers, Reston, Virginia. 1132 pp.
Garrels R. M. and Mackenzie F. T. (1971) *Evolution of Sedimentary Rocks.* Norton, New York. 397 pp.
Glotch T. D., Bandfield J. L., Christensen P. R., Calvin W. M., McLennan S. M., Clark B. C., Rogers A. D., and Squyres S. W. (2006) Mineralogy of the light-toned outcrop rock at Meridiani Planum as seen by the Miniature Thermal Emission Spectrometer and implications for its formation. *J. Geophys. Res., 111,* E12S03, DOI: 10.1029/2005JE002672.
Golden D. C., Ming D. W., Morris R. V., and Mertzmann S. M. (2005) Laboratory-simulated acid-sulfate weathering of basaltic materials: Implications for formation of sulfates at Meridiani Planum and Gusev crater, Mars. *J. Geophys. Res., 110,* E12S07, DOI: 10.1029/2005JE002451.
Goldhammer R. K., Dunn D. A., and Hardie L. A. (1987) High frequency glacio-eustatic sealevel oscillations with Milankovitch characteristics recorded in Middle Triassic platform carbonates in northern Italy. *Am. J. Sci., 287,* 853–892.
Goldich S. S. (1938) A study in rock weathering. *J. Geol., 46,* 17–58.
Golombek M. P., Grant J. A., Crumpler L. S., Greeley R., Arvidson R. E., Bell J. F. III, Weitz C. M., Sullivan R., Christensen P. R., Soderblom L. A., and Squyres S. W. (2006) Erosion rates at the Mars Exploration Rover landing sites and long-term climate change on Mars. *J. Geophys. Res., 111,* E12S10, DOI: 10.1029/2006JE002754.
Grant J. A. and Wilson S. A. (2011) Late alluvial fan formation in southern Margaritifer Terra, Mars. *Geophys. Res. Lett*., 38, L08201, DOI: 10.1029/2011GL046844.
Greeley R. and Iverson J. D. (1987) *Wind as a Geological Process on Earth, Mars, Venus, and Titan*. Cambridge Univ., Cambridge. 348 pp.
Greeley R., Bender K., Thomas P. E., Schubert G., Limonadi D., and Weitz C. M. (1995) Wind-related features and processes on Venus — Summary of Magellan results. *Icarus, 115,* 399–420.
Greeley R., Leach R. N., Williams S. H., Krinsley D. H., Marshall J. R., White B. R., and Pollack J. B. (1982) Rate of wind abrasion on Mars. *J. Geophys. Res., 87,* 10009–10024.
Grotzinger J. (2009) Beyond water on Mars. *Nature Geosci., 2,* 231–233.
Grotzinger J. P. and Milliken R. E. (2012) Sedimentary rock record of Mars: Distributions, origins, and global stratigraphy. In *Sedimentary Geology of Mars* (J. Grotzinger and R. Milliken, eds.), pp. 1–48. SEPM Spec. Publ. 102, Society for Sedimentary Geology, Tulsa.
Grotzinger J. P., Bell J. F. III, Calvin W., Clark B. C., Fike D., Golombek M., Greeley R., Herkenhoff K. E., Jolliff B., Knoll A. H., Malin M., McLennan S. M., and 6 colleagues (2005) Stratigraphy and sedimentology of a dry to wet eolian depositional system, Burns formation, Meridiani Planum, Mars. *Earth Planet. Sci. Lett., 240,* 11–72.
Grotzinger J., Bell J., Herkenhoff K., Johnson J., Knoll A., McCartney E., McLennan S., Metz J., Moore J., Squyres S., Sullivan R., Aharonson O., Arvidson R., Jolliff B., Golombek M., Lewis K., Parker T., and Soderblom J. (2006) Sedimentary textures formed by aqueous processes, Erebus crater, Meridiani Planum, Mars. *Geology, 34,* 1085–1088.
Grotzinger J., Beaty D., Dromart G., Gupta S., Harris M., Hurowitz J., Kocurek G., McLennan S., Milliken R., Ori G. G., and Sumner D. (2011) Mars sedimentary geology: Key concepts and outstanding questions. *Astrobiology, 11,* 77–87.
Grotzinger J. P., Crisp J., Vasavada A. R., Anderson R. C., Baker C. J., Barry R., Blake D. F., Conrad P., Edgett K. S., Ferdowski B., Gellert R., Golombek M., Gomez-Elvira J., Hassler D. M., Jandura L., Litvak M., Mahaffy P., Maki J., Meyer M., Malin M. C., Mitrofanov. I., Simmonds J. J., Vaniman D., Welch R. V., and Wiens R. (2012) Mars Science Laboratory Mission and science investigation. *Space Sci. Rev., 170,* 5–56.
Halevy I., Zuber M. T., and Schrag D. P. (2007) A sulfur dioxide climate feedback on early Mars. *Science, 318,* 1903–1907.
Hancock G. S., Anderson R. S., and Whipple K. X. (1998) Beyond power: Bedrock river incision process and form. In *Rivers Over Rock: Fluvial Processes in Bedrock Channels* (J. Tinkler and E. Wohl, eds.), pp. 35–60. AGU Geophys. Mono. 107, American Geophysical Union, Washington, DC.
Haskin L. A., Wang A., Jolliff B. L., McSween H. Y., Clark B. C., Des Marais D. J., McLennan S. M., and 23 colleagues (2005) Water alteration of rocks and soils on Mars at the Spirit rover site in Gusev crater. *Nature, 436,* 66–69.
Hayes A. G., Aharonson O., Callahan P., Elachi C., Gim Y., Kirk R., Lewis K., Lopes R., Lorenz R., Lunine J., Mitchell K., Mitri G., Stofan E., and Wall S. (2008) Hydrocarbon lakes on Titan: Distribution and interaction with a porous regolith. *Geophys. Res. Lett., 35,* L09204, DOI: 10.1029.2008GL033409.
Hayes A. G., Aharonson O., Lunine J. I., Kirk R. L., Zebker H. A., Wye L. C., Lorenz R. D., Turtle E. P., Paillou P., Mitri G., Wall S. D., Stofan E. R., Mitchell K. L., Elachi C., and the Cassini RADAR Team (2011a) Transient surface liquid in Titan's polar regions from Cassini. *Icarus, 211,* 655–671.
Hayes A. G., Grotzinger J. P., Edgar L. A., Squyres S. W., Watters W. A., and Sohl-Dickstein J. (2011b) Reconstruction of eolian bed forms and paleocurrents from cross-bedded strata at Victoria Crater, Meridiani Planum, Mars. *J. Geophys. Res., 16,* E00F21, DOI: 10.1029/2010JE003688.
Hayes A. G., Ewing R. C., Lucas A., McCormick C., Troy S., and Balard C. (2012) Determining the timescales of the dune forming winds on Titan. In *Third International Planetary Dunes Workshop: Remote Sensing and Data Analysis of Planetary*

Dunes, pp. 46–47. LPI Contribution No. 1673, Lunar and Planetary Institute, Houston.

Hayes A. G., Dietrich W. E. , Kirk R. L., Turtle E. P., Barnes J. W., Lucas A., and Mitchell K. L. (2013) Morphologic analysis of polar landscape evolution on Titan. In *Lunar Planet. Sci. XLIV,* Abstract #2000. Lunar and Planetary Institute, Houston.

Hecht M. H., Kounaves S. P., Quinn R. C., West S. J., Young S. M. M., Ming D. W., Catling D. C., Clark B. C., Boynton W. V., Hoffman J., DeFlores L. P., Gospodinova K., Kapit J., and Smith P. H. (2009) Detection of perchlorate and the soluble chemistry of martian soil at the Phoenix site. *Science, 325,* 64–67.

Hoffman P. F., Kaufman A. J., Halverson G. P., and Schrag D. P. (1998) A Neoproterozoic snowball Earth. *Science, 281,* 1342–1346.

Howard A. D., Dietrich W. E., and Seidl M. A. (1994) Modelling fluvial erosion on regional and continental scales. *J. Geophys. Res.–Solid Earth, 99,* 13971–13986.

Hurowitz J. A. and McLennan S. M. (2007) A ~3.5 Ga record of water-limited, acidic conditions on Mars. *Earth Planet. Sci. Lett., 260,* 432–443.

Hurowitz J. A., McLennan S. M., Lindsley D. H., and Schoonen M. A. A. (2005) Experimental epithermal alteration of synthetic Los Angeles meteorite: Implications for the origin of martian soils and the identification of hydrothermal sites on Mars. *J. Geophys. Res.–Planets, 110,* E07002, DOI: 10.1029/2004JE002391.

Hurowitz J. A., McLennan S. M., Tosca N. J., Arvidson R. E., Michalski J. R., Ming D. W., Schöder C., and Squyres S. W. (2006) In-situ and experimental evidence for acidic weathering on Mars. *J. Geophys. Res.–Planets, 111,* E02S19, DOI: 10.1029/2005JE002515.

Hynek B. M., Beach M., and Hoke M. R. T. (2010) Updated global map of martian valley networks and implications for climate anc hydrologic processes. *J. Geophys. Res.–Planets, 115,* E09008, DOI: 10.1029/2009JE003548.

Irwin R. P., Howard A. D., and Maxwell T. A. (2004) Geomorphology of Ma'adim Vallis, Mars, and associated paleolake basins. *J. Geophys. Res.–Planets, 109,* E12009, DOI: 10.1029/2004JE002287.

Iversen J. D. and White B. R. (1982) Saltation threshold on Earth, Mars and Venus. *Sedimentology, 29,* 111–119.

Iversen J. D., Greeley R., Marshall J. R., and Pollack J. B. (1987) Aeolian saltation threshold: The effect of density ratio. *Sedimentology, 34,* 699–706.

Janssen M. A., Lorenz R. D., West R., Paganelli F., Lopes R. M., Kirk R. L., Elachi C., Wall S. D., Johnson W. T. K., and Anderson Y. (2009) Titan's surface at 2.2-cm wavelength imaged by the Cassini RADAR radiometer: Calibration and first results. *Icarus, 200,* 222–239.

Jennings D. E., Flasar F. M., Kunde V. G., Samuelson R. E., Pearl J. C., Nixon C. A., Carlson R. C., Mamoutkine A. A., Brasunas J. C., Guandique E., Achterberg R. K., Bjoraker G. L., Romani P. N., Segura M. E., Albright S. A., Elliott M. H., Tingley J. S., Calcutt S., Coustenis A., and Courtin R. (2009) Titan's surface brightness temperatures. *Astrophys. J. Lett., 691,* L103.

Jennings D. E., Cottini V., Nixon C. A., Flasar F. M., Kunde V. G., Samuelson R. E., Romani P. N., Hesman B. E., Carlson R. C., Gorius N. J. P., Coustenis A., and Tokano T. (2011) Seasonal changes in Titan's surface temperatures. *Astrophys. J. Lett., 737,* L15, DOI: 10.1088/2041-8205/737/1/L15.

Jerolmack D. J. and Paola C. (2010) Shredding of environmental signals by sediment transport. *Geophys. Res. Lett., 37,* L19401, DOI: 10.1029/2010GL044638**.**

Johnson N. M. and Fegley B. Jr. (2002) Experimental studies of atmosphere-surface interactions on Venus. *Adv. Space Res., 29,* 233–241.

Johnsson M. J. (1993) The system controlling the composition of clastic sediments. In *Processes Controlling the Composition of Clastic Sediments* (M. J. Johnsson and A. Basu, eds.), pp. 1–19. Geol. Soc. Am. Spec. Paper 284, Geological Society of America, Boulder.

Johnsson M. J. and Meade R. H. (1990) Chemical weathering of fluvial sediments during alluvial storage: The Macuapanim Island pont bar, Solimoes River, Brazil. *J. Sed. Petrol., 60,* 827–842.

Jordan D. W. (1954) The adhesion of dust particles. *British J. Appl. Phys., 5,*194–198.

Kenyon P. M. and Turcotte D. L. (1985) Morphology of a delta prograding by bulk sediment transport. *Geol. Soc. Am. Bull., 96,* 1457–1465.

King P. L. and McLennan S. M. (2010) Sulfur on Mars. *Elements, 6,* 107–112.

Knauth L. P., Burt D. M., and Wohletz K. H. (2005) Impact origin of sediments at the Opportunity landing site on Mars. *Nature, 438,* 1123–1128.

Kocurek G. and Lancaster N. (1999) Aeolian system sediment state: Theory and Mojave desert Kelso dune field example. *Sedimentology, 46,* 505–515.

Kocurek G., Ewing R. C., and Mohrig D. (2010) How do bedform patterns arise? New views on the role of bedform interactions within a set of boundary conditions. *Earth Surf. Proc. Landforms, 35,* 51–63.

Komar P.D. (1980) Modes of sediment transport in channelized water flows with ramifications to the erosion of the martian outflow channels. *Icarus, 32,* 317–329.

Laity J. E. (2011) *Wind Erosion in Drylands,* pp. 539–568. John Wiley and Sons, Ltd.

Laity J. E. and Bridges N. T. (2009) Ventifacts on Earth and Mars: Analytical field, and laboratory studies supporting sand abrasion and windward feature development. *Geomorphology, 105,* 202–217.

Lamb M. P. and Dietrich W. E. (2009) The persistence of waterfalls in fractured rock. *Geol. Soc. Am. Bull., 121,* 1123–1134.

Lamb M. P. and Fonstad M. A. (2010) Rapid formation of a modern bedrock canyon by a single flood event. *Nature Geosci., 3,* 477–481.

Lamb M. P., Howard A. D., Johnson J., Whipple K. X., Dietrich W. E., and Perron J. T. (2006) Can springs cut canyons into rock? *J. Geophys. Res.–Planets, 111,* E07002, DOI: 10.1029/2005JE002663.

Lamb M. P., Dietrich W. E., Aciego S. M., DePaolo D. J., and Manga M. (2008a) Formation of Box Canyon, Idaho, by megaflood: Implications for seepage erosion on Earth and Mars. *Science, 320,* 1067–1070.

Lamb M. P., Dietrich W. E., and Sklar L. S. (2008b) A model for fluvial bedrock incision by impacting suspended and bed load sediment. *J. Geophys. Res.–Earth Surface, 113,* F03025, DOI: 10.1029/2007JF000915.

Lamb M. P., Dietrich W. E., and Venditti J. G. (2008c) Is the critical Shields stress for incipient sediment motion dependent on channel-bed slope? *J. Geophys. Res.–Earth Surface, 113,* F02008, DOI: 10.1029/2007JF000831.

Lamb M. P., Grotzinger J. P., Southard J. B., and Tosca N. J.

(2012) Were aqueous ripples on Mars formed by flowing brines? In *Sedimentary Geology of Mars* (J. Grotzinger and R. Milliken, eds.), pp. 139–150. SEPM Spec. Publ. 102, Society for Sedimentary Geology, Tulsa.

Leask H. J. and Wilson L. (2003) Heating and cooling of rocks on Mars: Consequences for weathering. In *Lunar Planet. Sci. XXXIV,* Abstract #1804, Lunar and Planetary Institute, Houston.

Le Gall A., Janssen M. A., Paillou P., Lorenz R. D., and Wall S. D. (2010) Radar-bright channels on Titan. *Icarus, 207,* 948–958.

Le Gall A., Hayes A. G., Ewing R., Janssen M. A., Radebaugh J., Savage C., Encrenaz P., and the Cassini RADAR Team (2012) Latitudinal and altitudinal controls of Titan's dune field morphometry. *Icarus, 217,* 231–242.

Lewis K. W., Aharonson O., Grotzinger J. P., Kirk R. L., McKewan A. S., and Suer T.-A. (2008) Quasi-periodic bedding in the sedimentary rock record of Mars. *Science, 322,* 1532–1535.

Litwin K. L., Zygielbaum B. R., Polito P. J., Sklar L. S., and Collins G. C. (2012) Influence of temperature, composition, and grain size on the tensile failure of water ice: Implications for erosion on Titan. *J. Geophys. Res.–Planets, 117,* E08013, DOI: 10.1029/2012JE004101.

Lopes R. M. C., Stofan E. R., Peckyno R., Radebaugh J., Mitchell K. L., Mitri G., Wood C. A., Kirk R. L., Wall S. D., Lunine J. I., Hayes A., Lorenz R., Farr T., Wye L., Craig J., Ollerenshaw R. J., Janssen M., Legall A., Paganelli F., West R., Stiles B., Callahan P., Anderson Y., Valora P., Soderblom L., and the Cassini RADAR Team (2010) Distribution and interplay of geologic processes on Titan from Cassini radar data. *Icarus, 205,* 540–558.

Lopes R. M. C., Kirk R. L., Michell K. L., LeGall A., Barnes J. W., Hayes A. G., Kargel J., Wye L., Radebaugh J., Stofan E. R., Janssen M. A., Neish C. D., Wall S. D., Wood C. A., Lunine J. I., and Malaska M. (2013) Cryovolcanism on Titan: New results from the Cassini RADAR and VIMS. *J. Geophys. Res.–Planets,* in press.

Lorenz R. D. and Lunine J. I. (1996) Erosion on Titan: Past and present. *Icarus, 122,* 79–91.

Lorenz R. D. and Lunine J. I. (2005) Titan's surface before Cassini. *Planet. Space Sci., 53,* 557–576.

Lorenz R. D., McKay C. P., and Lunine J. I. (1997) Photochemically induced collapse of Titan's atmosphere. *Science, 275,* 642–644.

Lorenz R. D., Wall S., Radebaugh J., Boubin G., Reffet E., Janssen M., Stofan E., Lopes R., Kirk R., Elachi C., Lunine J., Mitchell K., Paganelli F., Soderblom L., Wood C., Wye L., Zebker H., Anderson Y., Ostro S., Allison M., Boehmer R., Callahan P., Encrenaz P., Ori G. G., Francescetti G., Gim Y., Hamilton G., Hensley S., Johnson W., Kelleher K., Muhleman D., Picardi G., Posa F., Roth L., Seu R., Shaffer S., Stiles B., Vetrella S., Flamini E., and West R. (2006) The sand seas of Titan: Cassini RADAR observations of longitudinal dunes. *Science, 312,* 724–727.

Lorenz R. D., Lopes R. M., Paganelli F., Lunine J. I., Kirk R. L., Mitchell K. L., Soderblom L. A., Stofan E. R., Ori G., Myers M., Miyamoto H., Radebaugh J., Stiles B., Wall S. D., and Wood C. A. (2008) Fluvial channels on Titan: Initial Cassini RADAR observations. *Planet. Space Sci., 56,* 1132–1144.

Lorenz R. D., Newman J. I., and Lunine J. I. (2010) Threshold of wave generation on Titan's lakes and seas: Effects of viscosity and implications for Cassini observations. *Icarus, 207,* 932–937.

Lunine J. I. and Atreya S. (2008) The methane cycle on Titan. *Nature Geosci., 1,* 159–164.

Malin M. C. (1974) Salt weathering on Mars. *J. Geophys. Res., 79,* 3888–3894.

Malin M. C. (1986) Rates of geomorphic modification in ice-free areas, southern Victoria Land, Antarctica. *Antarctic J. U.S., 20,* 18–21.

Mangold N., Quantin C., Ansan V., Delacourt C., and Allemand P. (2004) Evidence for precipitation on Mars from dendritic valleys in the Valles Marineris Area. *Science, 305,* 78–81.

McCollom T. M. and B. M. Hynek (2005) A volcanic environment for bedrock diagenesis at Meridiani Planum on Mars. *Nature, 438,* 1129–1131.

McGlynn I. O., Fedo C. M., and McSween H. Y. (2012) Soil mineralogy at the Mars Exploration Rover landing sites: An assessment of the competing roles of physical sorting and chemical weathering. *J. Geophys. Res., 117,* E01006, DOI: 10.1029/2010JE003712.

McKee E. D. (1979) *A Study of Global Sand Seas*. U.S. Geol. Surv. Prof. Paper 1052, U.S. Govt. Printing Office, Washington, DC. 429 pp.

McLennan S. M. (2003) Sedimentary silica on Mars. *Geology, 31,* 315–318.

McLennan S. M. (2012) Geochemistry of sedimentary processes on Mars. In *Sedimentary Geology of Mars* (J. P. Grotzinger and R. E. Milliken, eds.) pp. 119–138. SEPM Spec. Publ. 102, Society for Sedimentary Geology, Tulsa.

McLennan S. M. and Grotzinger J. P. (2008) The sedimentary rock cycle of Mars. In *The Martian Surface: Composition, Mineralogy, and Physical Properties* (J. F. Bell III, ed.), pp. 541–577. Cambridge Univ., Cambridge.

McLennan S. M., Bell J. F. III, Calvin W., and 29 colleagues (2005) Provenance and diagenesis of the evaporite-bearing Burns formation, Meridiani Planum, Mars. *Earth Planet. Sci. Lett., 240,* 95–121.

McSween H. Y., McGlynn I. O., and Rogers A. D. (2010) Determining the modal mineralogy of martian soils. *J. Geophys. Res., 115,* E00F12, DOI: 10.1029/2010JE003582.

Melosh H. J. (2011) *Planetary Surface Processes.* Cambridge Univ., New York. 500 pp.

Metz J. M., Grotzinger J., Rubin D. M., Lewis K. W., Squyres S. W., and Bell J. F. III (2009) Sulfate-rich eolian and wet interdune deposits, Erebus crater, Meridiani Planum, Mars. *J. Sed. Res., 79,* 247–264.

Miller M. C., McCave I. N., and Komar P. D. (1977) Threshold of sediment motion under unidirectional currents. *Sedimentology, 41,* 883–903.

Milliken R.E. and Bish D.L. (2010) Sources and sinks of clay minerals on Mars. *Philos. Mag., 90,* 2293–2308.

Milliken R. E., Grotzinger J. P., and Thompson B. J. (2010) Paleoclimate of Mars as captured by the stratigraphic record in Gale Crater. *Geophys. Res. Lett., 37,* L04201, DOI: 10.1029/2009GL041870.

Millot R., Gaillardet J., Dupré B., and Allègre C. J. (2002) The global control of silicate weathering rates and the coupling with physical erosion: New insights from rivers of the Canadian Shield. *Earth Planet. Sci. Lett., 196,* 83–98.

Ming D. W., Mittlefehldt D. W., Morris R. V., Golden D. C., Gellert R., Yen A., Clark B. C., Squyres S. W., Farrand W. H., Ruff S. W., Arvidson R. E., Klingelhöfer G., McSween H. Y., Rodionov D. S., Schröder C., de Souza P. A., and Wang A. (2006) Geochemical and mineralogical indicators for aqueous processes in the Columbia Hills of Gusev crater, Mars. *J.*

Geophys. Res., 111, E02S12, DOI: 10.1029/2005JE002560.

Mitchell K. L. and Malaska M. (2011) Karst on Titan. In *First International Planetary Caves Workshop: Implications for Astrobiology, Climate, Detection, and Exploration,* p. 15. LPI Contribution No. 1640, Lunar and Planetary Institute, Houston.

Mitchell K. L., Kargel J. S., Wood C. A., Radebaugh J., Lopes R. M. C., Lunine J. I., Stofan E. R., Kirk R. L., and the Cassini RADAR Team (2007) Titan's crater lakes: Caldera vs. karst. In *Lunar Planet. Sci. XXXVIII,* Abstract #2064. Lunar and Planetary Institute, Houston.

Montgomery D. R. and Buffington J. M. (1997) Channel-reach morphology in mountain drainage basins. *Geol. Soc. Am. Bull., 109,* 596–611.

Moore J. M and Howard A. D. (2010) Are the basins of Titan's Hotei Regio and Tui Regio sites of former low latitude seas? *Geophys. Res. Lett., 37,* L22205, DOI: 10.1029/2010GL046753.

Moore J. M. and Pappalardo R. T. (2011) Titan: An exogenic world? *Icarus, 212,* 790–806.

Morris R. V., Ruff S. W., Gellert R., Ming D. W., Arvidson R. E., Clark B. C., Golden D. C., Siebach K., Klingelhöfer G., Schroder C., Fleischer I., Yen A. S., and Squyres S. W. (2010) Identification of carbonate-rich outcrops on Mars by the Spirit rover. *Science, 329,* 421–424.

Murchie S. L., Mustard J. F., Ehlmann B. L., Milliken R. E., Bishop J. L., McKeown N. K., Noe Dobrea E. Z., Seelos F. P., Buczkowski D. L., Wiseman S. M., Arvidson R. E., Wray J. J., Swayze G., Clark R. N., Des Marais D. J., McEwen A. S., and Bibring J.-P. (2009) A synthesis of martian aqueous mineralogy after 1 Mars year of observations from the Mars Reconnaissance Orbiter. *J. Geophys. Res.–Planets, 114,* E00D06, DOI: 10.1029/2009JE003342.

Navarre-Sitchler A. and Brantley S. (2007) Basalt weathering across scales. *Earth Planet. Sci. Lett., 261,* 321–334.

Neish C. D., Kirk R. L., Lorenz R. D., Bray V., Schenk P., Stiles B., Turtle E. P., Mitchell K., and Hayes A. G. (2013) Crater topography on Titan: Implications for landscape evolution. *Icarus, 223(1),* 82–90, DOI: 10.1016/j.icarus.2012.11.030.

Nelson R. M., Kamp L. W., Matson D. L., Irwin P. G. J., Baines K. H., Boryta M. D., Leader F. E., Jaumann R., Smythe W. D., Sotin C., Clark R. N., Cruikshank D. P., Drossart P., Pearl J. C., Hapke B. W., Lunine J., Combes M., Bellucci G., Bibring J.-P., Capaccioni F., Cerroni P., Coradini A., Formisano V., Filacchione G., Langevin R. Y., McCord T. B., Mennella V., Nicholson P. D., and Sicardy B. (2009) Saturn's Titan: Surface change, ammonia, and implications for atmospheric and tectonic activity. *Icarus, 199,* 429–441.

Nesbitt H. W. (1997) Bacterial and inorganic weathering processes and weathering of crystalline rocks. In *Biological-Mineralogical Interactions* (J. M. McIntosh and L. A. Grout, eds.), pp. 113–142. Mineralogical Association of Canada Short Course Series 25.

Nesbitt H. W. (2003) Petrogenesis of siliciclastic sediments and sedimentary rocks. In *Geochemistry of Sediments and Sedimentary Rocks: Evolutionary Considerations to Mineral Deposit-Forming Environments* (D. R. Lentz, ed.), pp. 39–51. Geol. Assoc. Canada GeoText, Vol. 4.

Nesbitt H. W. and Markovics G. (1997) Weathering of granodioritic crust, long-term storage of elements in weathering profiles, and petrogenesis of siliciclastic sediments. *Geochim. Cosmochim. Acta, 61,* 1653–1670.

Nesbitt H. W. and Wilson R. E. (1992) Recent chemical weathering of basalts. *Am. J. Sci., 292,* 740–777.

Nesbitt H. W. and Young G. M. (1984) Prediction of some weathering trends of plutonic and volcanic rocks based on thermodynamic and kinetic considerations. *Geochim. Cosmochim. Acta, 48,* 1523–1534.

Nickling W. G. and Neuman C. M. (2009) *Aeolian Sediment Transport,* pp. 539–568. Springer, Berlin.

Niemann H. B., Atreya S. K., Bauer S. J., Carignan G. R., Demick J. E., Frost R. L., Gautier D., Haberman J. A., Harpold D. N., Hunten D. M., Israel G., Lunine J. I., Kasprzak W. T., Owen T. C., Paulkovich M., Raulin F., Raaen E., and Way S. H. (2005) The abundances of constituents of Titan's atmosphere from the GCMS instrument on the Huygens probe. *Nature, 438,* 779–784.

Nikuradse J. (1933) Stromungsgesetze in rauhen Rohren. *Forschung auf dem Gebiete des Ingenieurwesens, Forschungsheft 361.* VDI Verlag, Berlin, Germany (in German). (Translated in *Laws of Flow in Rough Pipes,* NACA TM 1292, National Advisory Committee for Aeronautics, Washington, DC, 1950).

Nino Y., Lopez F., and Garcia M. (2003) Threshold for particle entrainment into suspension. *Sedimentology, 50,* 247–263.

Nishimura K. and Hunt J. C. R. (2000) Saltation and incipient suspension above a at particle bed below a turbulent boundary layer. *J. Fluid Mech., 417,* 77–102.

Nittler L. R., Starr R. D., Weider S. Z., McCoy T. J., Boynton W. V., Ebel D. S., Ernst C. M., Evans L. G., Goldstein J. O., Hamara D. K., Lawrence D. J., McNutt R. L., Schlemm C. E., Solomon S. C., and Sprague A. L. (2011) The major-element composition of Mercury's surface from MESSENGER X-ray spectrometry. *Science, 333,* 1847–1850.

Oelkers E. H. and Schott J., eds. (2009) *Thermodynamics and Kinetics of Water-Rock Interaction.* Rev. Mineral. Geochem., Vol. 70. 569 pp.

O'Hara-Dhand K., Taylor R. L. S., Smalley I. J., Krinsley D. H., and Vita- Finzi C. (2010) Loess and dust on Earth and Mars: Particle generation by impact mechanisms. *Central European J. Geosci., 2,* 45–51.

Pain C. F., Clarke J. D. A., and Thomas M. (2007) Inversion of relief on Mars. *Icarus, 190,* 478–491.

Paola C. (2000) Quantitative models of sedimentary basin filling. *Sedimentology, 47, Suppl. 1,* 121–178.

Paola C. and Voller V. R. (2005) A generalized Exner equation for sediment mass balance. *J. Geophys. Res.–Earth Surface, 110,* F04014, DOI: 10.1029/2004JF000274.

Parker G. (1990) Surface-based bedload transport relation for gravel rivers. *J. Hydr. Res., 28,* 417–436.

Parker G. (1991) Selective sorting and abrasion of river gravel. II: Applications. *J. Hydr. Engin., 117,* 150–171.

Parker G., Wilcock P. R., Paola C., Dietrich W. E., and Pitlick J. (2007) Physical basis for quasi-universal relations describing bankfull hydraulic geometry of single-thread gravel bed rivers. *J. Geophys. Res.–Earth Surface, 112,* F04005, DOI: 10.1029/2006JF000549.

Pelletier J. D., Cline M., and Delong S. B. (2007) Desert pavement dynamics: Numerical modeling and field-based calibration. *Earth Surf. Proc. Landforms, 32,* 1913–1927.

Perron J. T., Lamb M. P., Koven C. D., Fung I. Y., Yager E., and Adamkovics M. (2006) Valley formation and methane precipitation rates on Titan. *J. Geophys. Res.–Planets, 111,* E11001, DOI: 10.1029/2005JE002602.

Pye K. (1987) *Aeolian Dust and Dust Deposits.* Academic, London.

Rubin D. M. and Hesp P. A. (2009) Multiple origins of linear dunes

on Earth and Titan. *Nature Geosci., 2,* 653–658.
Rubin D. M. and Hunter R. E. (1987) Bedform alignment in directionally varying flows. *Science, 237,* 276–278.
Schlichting H. (1979) *Boundary-Layer Theory*. McGraw-Hill, New York. 817 pp.
Schneider T., Graves S. D. B., Schaller E. L., and Brown M. E. (2012) Polar methane accumulation and rainstorms on Titan from simulations of the methane cycle. *Nature, 481,* 58–61.
Schröder S. and Keller H. (2008) The reflectance spectrum of Titan's surface at the Huygens landing site determined by the descent imager/spectral radiometer. *Planet. Space Sci., 56,* 753–769.
Selivanov A. S., Gektin Yu. M., Naraeva M. K., Panfilov A. S., and Fokin A. B. (1982) Evolution of the Venera 13 imagery. *Sov. Astron. Lett., 8,* 235–237.
Shao Y. and Lu H. (2000) A simple expression for wind erosion threshold friction velocity. *J. Geophys. Res., 105,* 22437–22444.
Sharp R. P. and Malin M. C. (1975) Channels on Mars. *Geol. Soc. Am. Bull., 86,* 593–609.
Shields A. (1936) *Application of Similarity Principles and Turbulence Research to Bed-Load Movement*. U.S. Dept. of Agriculture Soil Conservation Service Cooperative Laboratory, California Institute of Technology, Pasadena.
Sklar L.S. (2012) Erodibility of Titan ice bedrock constrained by laboratory measurements of ice strength and erosion by sediment impacts. *AGU Fall Meeting,* Abstract #EP44A-06.
Sklar L. S. and Dietrich W. E. (2001) Sediment and rock strength controls on river incision into bedrock. *Geology, 29,* 1087–1090.
Sklar L. S. and Dietrich W. E. (2004) A mechanistic model for river incision into bedrock by saltating bed load. *Water Resour. Res., 40,* W06301, DOI: 10.1029/2012WR012267.
Soderblom L. A., Kirk R. L., Lunine J. I., Anderson J. A., Baines K. H., Barnes J. W., Barrett J. M., Brown R. H., Buratti B. J., Clark R. N., Cruikshank D. P., Elachi C., Janssen M. A., Jaumann R., Karkoschka E., Mouélic S. L., Lopes R. M., Lorenz R. D., McCord T. B., Nicholson P. D., Radebaugh J., Rizk B., Sotin C., Stofan E. R., Sucharski T. L., Tomasko M. G., and Wall S. D. (2007) Correlations between Cassini VIMS spectra and ADAR SAR images: Implications for Titan's surface composition and the character of the Huygens probe landing site. *Planet. Space Sci., 55,* 2025–2036.
Sotin C., Mielke R., Choukroun M., Neish C., Barmatz M., Castillo J., Lunine J., and Mitchell K. (2009) Ice-hydrocarbon interactions under Titan-like conditions: Implications for the carbon cycle on Titan. In *Lunar Planet. Sci. XL,* Abstract #2088. Lunar and Planetary Institute, Houston.
Southard J. B. (1991) Experimental determination of bed-form stability. *Annu. Rev. Earth Planet. Sci., 19,* 423–455.
Southard J. B. and Boguchwal L. A. (1990a) Bed configurations in steady unidirectional water flows. 2. Synthesis of flume data. *J. Sed. Petrol., 60,* 658–679.
Southard J. B. and Boguchwal L. A. (1990b) Bed configurations in steady unidirectional water flows. 3. Effects of temperature and gravity. *J. Sed. Petrol., 60,* 680–686.
Squyres S. W., Grotzinger J. P., Arvidson R. E., Bell J. F. III, Christensen P. R., Clark B. C., Crisp J. A., Farrand W. H., Herkenhoff K. E., Johnson J. R., Klingelhöfer G., Knoll A. H., McLennan S. M., and 5 colleagues (2004) In-situ evidence for an ancient aqueous environment on Mars. *Science, 306,* 1709–1714.
Stefannsson A. and Gislason S. (2001) Chemical weathering of basalts, southwest Iceland: Effect of rock crystallinity and secondary minerals on chemical fluxes to the ocean. *Am. J. Sci., 301,* 513–556.
Sullivan R., Arvidson R., Bell J. F., Gellert R., Golombek M., Greeley R., Herkenhoff K., Johnson J., Thompson S., Whelley P., and Wray J. (2008) Wind-driven particle mobility on Mars: Insights from Mars Exploration Rover observations at El Dorado and surroundings at Gusev Crater. *J. Geophys. Res., 113,* E06S07, DOI: 10.1029/2008JE003101.
Surkov Yu. A., Barsukov V. L., Moskalyeva L. P., Kharyukova V. P., and Kemurdzhian A. L. (1984) New data on the composition, structure, and properties of Venus rock obtained by Venera 13 and Venera 14. *Proc. Lunar Planet. Sci. Conf. 14th, Part 2, J. Geophys. Res., 89,* B393–B402.
Surkov Yu. A., Moskalyeva L. P., Kharyukova V. P., Dudin A. D., Smirnov G. G., and Zaitseva S. Ye. (1986) Venus rock composition at the Vega 2 landing site. *Proc. Lunar Planet. Sci. Conf. 17th, Part 1, J. Geophys. Res., 91,* E215–E218.
Surkov Yu. A., Kirnozov F. F., Glazov V. N., Dunchenko A. G., Tatsy L. P., and Sobornov O. P. (1987) Uranium, thorium, and potassium in the venusian rocks at the landing sites of Vega 1 and 2. *Proc. Lunar Planet. Sci. Conf. 17th, Part 2, J. Geophys. Res., 92,* E537–E540.
Taylor G. J., McLennan S. M., McSween H. Y., Wyatt M. B., and Lentz R. C. F. (2008) Implications of observed primary lithologies. In *The Martian Surface: Composition, Mineralogy, and Physical Properties* (J. F. Bell III, ed.), pp. 501–518. Cambridge Univ., Cambridge.
Taylor S. R. and McLennan S. M. (1985) *The Continental Crust: Its Composition and Evolution.* Blackwell, Oxford. 312 pp.
Taylor S. R. and McLennan S. M. (2009) *Planetary Crusts: Their Composition, Origin, and Evolution.* Cambridge Univ., Cambridge. 378 pp.
Tobie G., Lunine J., and Sotin C. (2006) Episodic outgassing as the origin of atmospheric methane on Titan. *Nature, 440,* 61–64.
Tomasko M. G., Archinal B., Becker T., Bézard B., Bushroe M., Combes M., Cook D., Coustenis A., de Bergh C., Dafoe L. E., Doose L., Douté S., Eibl A., Engel S., Gliem F., Grieger B., Holso K., Howington-Kraus A., Karkoschka E., Keller H. U., Kirk R., Kramm R., Kuppers M., Lellouch E., Lemmon M., Lunine J., McFarlane E., Moores J., Prout M., Rizk B., Rosiek M., Ruffer P., Schroeder S., Schmitt B., See C., Smith P., Soderblom L., Thomas N., and West R. (2005) Rain, wind, and haze during the Huygens probe's descent to Titan's surface. *Nature, 438,* 765–778.
Tosca N. J. and McLennan S. M. (2006) Chemical divides and evaporite assemblages on Mars. *Earth Planet. Sci. Lett., 241,* 21–31.
Tosca N. J., McLennan S. M., Lindsley D. H., and Schoonen M. A. A. (2004) Acid-sulfate weathering of synthetic martian basalt: The acid fog model revisited. *J. Geophys. Res., 109,* E05003, DOI: 10.1029/2003JE002218.
Tosca N. J., McLennan S. M., and 6 colleagues (2005) Geochemical modeling of evaporation processes on Mars: Insight from the sedimentary record at Meridiani Planum. *Earth Planet. Sci. Lett., 240,* 122–148.
Tosca N. J., McLennan S. M., Lamb M. P., and Grotzinger J. P. (2011) Physicochemical properties of concentrated martian surface waters. *J. Geophys. Res.–Planets, 116,* E05004, DOI: 10.1029/2010JE003700.
Tsoar H. and Pye K. (1987) Dust transport and the question of desert loess formation. *Sedimentology, 34,* 139–153.

Turtle E. P., Perry J. E., Hayes A. G., Lorenz R. D., Barnes J. W., McEwen A. S., West R. A., Ray T. L., Del Genio A. D., Barbara J. M., and Schaller E. L. (2011) Extensive and rapid surface changes near Titan's equator: Evidence for April showers? *Science, 18,* 331.

Ungar J. E. and Haff P. K. (1987) Steady state saltation in air. *Sedimentology, 34,* 289–299.

van den Berg J. H. and van Gelder A. (1993) A new bedform stability diagram, with emphasis on the transition of ripples to plane bed in flows over fine sand and silt. *Spec. Publ. Intern. Assoc. Sediment., 17,* 11–21.

van der Weijden C. H., and Pacheco F. A. L. (2003) Hydrochemistry, weathering and weathering rates on Madeira Island. *J. Hydrol., 283,* 122–145.

Veizer J. and Mackenzie F. T. (2003) Evolution of sedimentary rocks. In *Treatise on Geochemistry, Vol. 7: Sediments, Diagenesis, and Sedimentary Rocks* (F. T. Mackenzie, ed.), pp. 369–407. Elsevier-Pergamon, Oxford.

Viles H., Ehlmann B., Wilson C. F., Cebula T., Page M., and Bourke M. (2010) Simulating weathering of basalt on Mars and Earth by thermal cycling. *Geophys. Res. Lett., 37,* L18201, DOI: 10.1029/2010GL043522.

Wall S., Hayes A., Bristow C., Lorenz R., Stofan E., Lunine J., Le Gall A., Janssen M., Lopes R., Wye L., Soderblom L., Paillou P., Aharonson O., Zebker H., Farr T., Mitri G., Kirk R., Mitchell K., Notarnicola C., Casarano D., and Ventura B. (2010) Active shoreline of Ontario Lacus, Titan: A morphological study of the lake and its surroundings. *Geophys. Res. Lett., 37,* L05252, DOI: 10.1029/2009GL041821.

Warner N. H., Gupta S., Kim J. R., Lin S. Y., and Muller J. P. (2010) Retreat of a giant cataract in a long-lived (3.7–2.6 Ga) martian outflow channel. *Geology, 38,* 791–794.

Warren J. K. (2010) Evaporites through time: Tectonic, climatic, and eustatic controls in marine and nonmarine deposits. *Earth-Sci. Rev., 98,* 217–268.

Werner B. T. and Kocurek G. (1999) Bedform spacing from defect dynamics. *Geology, 27,* 727–730.

West A. J., Galy A., and Bickle M. (2005) Tectonic and climatic controls on silicate weathering. *Earth Planet. Sci. Lett., 235,* 211–228.

Whipple K. X. (2004) Bedrock rivers and the geomorphology of active orogens. *Annu. Rev. Earth Planet. Sci., 32,* 151–185.

Whipple K. X., Hancock G. S., and Anderson R. S. (2000) River incision into bedrock: Mechanics and relative efficacy of plucking, abrasion, and cavitation. *Geol. Soc. Am. Bull., 112,* 490–503.

White A. F. (1995) Chemical weathering rates of silicate minerals in soils. *Rev. Mineral., 31,* 407–461.

White A. F. and Brantley S. L., eds. (1995) *Chemical Weathering Rates of Silicate Minerals.* Rev. Mineral., Vol. 31. 583 pp.

White S. J. (1970) Plane bed thresholds of fine grained sediments. *Nature, 228,* 152–153.

Wilcock P. R. (1993) Critical shear-stress of natural sediments. *J. Hydrol. Eng., 119,* 491–505.

Wilcock P. R. and Crowe J. C. (2003) Surface-based transport model for mixed-size sediment. *J. Hydrol. Eng., 129,* 120–131.

Williams R. M. E. and Malin M. C. (2004) Evidence for late stage fluvial activity in Kasei Valles, Mars. *J. Geophys. Res., 109,* E06001, DOI: 10.1029/2003JE002178.

Wood C. A., Lorenz R., Kirk R., Lopes R., Mitchell K., and Stofan E. (2010) Impact craters on Titan. *Icarus, 206,* 334–344.

Yarger J., Lunine J. I., and Burke M. (1993) Calorimetric studies of the ammonia-water system with application to the outer solar system. *J. Geophys. Res., 98,* 13109–13117.

Yung Y. L., Allen M., and Pinto J. P. (1984) Photochemistry of the atmosphere of Titan — Comparison between model and observations. *Astrophys. J., 55,* 465–506.